12-2014

Effect of Thermal Treatments on Mechanical Properties and Bioactivity of Third Generation of Bioactive Glass. A step for commercialization success of third Generation Bioactive Glasses

Rajan Pandya

Effect of Thermal Treatments on Mechanical Properties and Bioactivity of Third Generation of Bioactive Glass.

A step for commercialization success of third Generation Bioactive Glasses

by

RAJAN PANDYA

Bachelor of Technology, Ganpat University, India

a thesis submitted to the Department of Biomedical Engineering

of Florida Institute of Technology in partial fulfilment

of the requirement for the degree of

MASTER OF SCIENCE

In

BIOMEDICAL ENGINEERING

Melbourne, Florida

December 2014

Effect of Thermal Treatments on Mechanical Properties and Bioactive Glass of Third Generation of Bioactive Glass.

A step for commercialization success of third Generation Bioactive Glasses

A THESIS

by

RAJAN PANDYA

Approved as to style and content by:

Dr. Michael Fenn, Ph. D., Chairperson Professor, Department of Biomedical Engineering	Dr. Vipuil Kishore, Ph.D., Member Professor, Department of Chemical Engineering
Dr. Mehmet Kaya, Ph.D., Member Professor, Department of Biomedical Engineering	Dr. Ted Conway, Ph.D., Department Head, Department of Biomedical Engineering

ACKNOWLEDGEMENTS

First of all I would like to thank Dr. Larry L. Hench. I cannot find enough words to express how much I have learnt from him over the past two years. I feel, his help has made me more aware of how the things work in the real world and prepared for all the challenges I may face in coming years. I would like to thank my adviser Dr. Michael Fenn for the wonderful opportunity to work on the project for my thesis. I wouldn't have come where I am without all the guidance and knowledge he shared with me during my thesis process. Not only is he my mentor but also an invaluable support who I could turn to, anytime I had to. I am also indebted to my committee members, Dr. Mehmet Kaya and Dr. Vipuil Kishore. Their support and constructive criticism helped me improve the quality of my research throughout. I would also like thank Florida Institute of Technology for accepting me in this graduate program and providing funding for my research through the research assistantship.

I would like to thank our ex-department head Dr. Kunal Mitra for his guidance during the initial parts of thesis work. I would like to sincerely thank our department head Dr. Ted Conway for being supportive and encouraging. I would also like to thank Thuy-Uyen Nguyen for helping me with biocompatibility test for my materials, and I would also like to thank Eric Mason, who helped and assisted me in sintering treatments I performed. I would also like to extend my gratitude towards Maxime Michael for helping me with the instruments that I had to use during my experiments and Karen Hart for her support.

ABSTRACT

Unavailability of donors for transplanting bone to help people with orthopedic imparities gave rise to the metal implants that could be made in factories. This seemed like a good solution as it was available to all the people who needed it. It came with limitations such as restricted movement, infection, wear and tear of the surrounding tissue, and rejection. Biologically active implants were introduced by Dr. Larry Hench in 1960s [12]. The field of regenerative medicine has been changing rapidly since then. Biologically active implants facilitate bone regeneration and do not harm the surrounding tissue in any way. The bioactive glasses when supplied with the growth factors help the tissue to regenerate strength of the new tissue formed is almost equal to and in some cases greater than the natural tissue. There are many variables that affect or enhance the strength and biological activity of the bioactive glasses. Some of these variables are: composition of the bioactive implant, temperature used in sintering, time of exposure. In this study we looked at effect of sintering temperature and exposure time on mechanical strength and bioactivity of the bioactive glass. It was found that, as the sintering temperature and exposure time increased the materials that were produced were more strong and biocompatible.

Table of Contents

List of Tables

List of Figures

LIST OF ABBREVIATIONS

Hap/HA: Hydroxyapatite

BMP: Bone Morphogenetic Proteins

TGF-β: Transforming growth factor β

IGF I and II: Insulin like growth factors I and II

PDGF: Platelet Derived Growth Factor basic and

bFGF: basic Fibroblast Growth Factor

aFGF: acidic Fibroblast Growth Factor

TCP: Tri Calcium Phosphate

SBF: Simulated Body Fluid

HCA: Hydroxyl Carbonate Apatite

HCFA: Hydroxyl fluroapatite

DTA: Differential Thermal Analysis

SEM: Scanning Electron Microscope

MPa: Mega Pascal

Chapter 1: Introduction and Hypothesis

Discovery of bioceramics in 1970 revolutionized the field of biomaterials. Prior to that people had to rely on orthopedic transplants or prosthetics in case of loss of organ of the body [1, 2]. Advent of the field of bioceramics led to an era of tissue engineering and regenerative medicine to enhance the natural process of the body [3].

Tissue engineering is one of the fastest advancing fields; it gives us a better approach for either repairing or regenerating the tissues or organs lost due to trauma, injury, disease, or aging [4]. Unlike the old times when people had to rely on available living tissue for transplant, tissue scaffolds can be synthesized using biomaterials, growth factors, other biomolecules, along with the cells. The growth factors and biomolecules guide and regulate the growth of cells around the scaffold there by, eliminating the necessity of surgery [5-7]. This is regenerative medicine, the very first study done on regeneration, was done on tracheal cells where a 78 year old woman suffering from thyroid cancer was implanted with scaffold and cells. They observed that tracheal luminal surface was gradually being covered with new epithelial cells after 2 months. This growth continued till two years without any complications [8].

The growth factors and proteins that need to be supplied are an expensive process and become difficult after implanting the scaffold. Today, engineers have come up with a technique that involves genetic activation that leads

the stem cells to make the required proteins for cartilage regeneration [9]. These advances would not have been done without the innovative design and fabrication of biomaterials. Scaffold designed using new techniques follow the stringent requirements depending on what tissue needs to be regenerated [11].

There are two categories of the bone scaffold. First one is human tissue derived of scaffold. These can be homologous cancellous or deminerialized [12]. Second category of the bone scaffolds is the medicinal devices that are biomaterial scaffolds. The bioactive scaffolds not only provide a 3D structure to the damaged tissue but also allow tissue growth at the interface. The biomaterials used in regenerative medicine also have a huge variety. Some of them are discussed here, Polymers: can be natural (collagen, fibrin, and hyaluronic acid) or synthetic (polypropylene fumarate, polycaprolactones, and polyactide) [13]. They have good osteoconduction and really good compatibility. Mechanical properties, physical attributes, and degradation time of the synthetic polymer are different for each synthetic polymer [14, 15]. Even with these advantages, polymers are not a perfect choice because of poor mechanical properties.

Metallic biomaterials are also frequently used in surgeries of orthopedic and dental surgeries. The metals used are stainless steel 316L, Cobalt-chromium alloy, cobalt based alloys, and titanium based alloys [16]. The metal implants, unlike polymers, have very high mechanical strength but they are very less bio-compatible. They sometimes even release toxic ions in the human body. The toxic ions cause inflammatory response [17]. Other material used in the

orthopedic or dental surgery is ceramic. These are non metallic and non organic materials. They have very high compressive strength. In this study, we used water quenched bioactive glasses and studied effect of heat on their mechanical strength and compatibility.

Discovery of bio-glass is the remarkable event that set a turning point in bioceramics field. First biologically relevant bioactive glass composition was made by Dr. Larry Hench and his colleagues at University of Florida [19]. Inspired by the question," If you can make a material that will survive exposure to high energy radiation can you make a material that will survive exposure to the human body?"[18], Dr. Larry Hench and his team submitted a research proposal to the US army that would study the materials that would be used in place of metal or plastic implants [18].

There are three generations of bioactive glass so far. The first generation of bioglass is used just to replace the damaged tissue. The bioglass implants in this generation are inert and cause minimal scarring of tissue surrounding it. More than 50 types of implants made from 40 different first generation biomaterials were used annually to help people in distress [20]. The second generation bioactive glasses had a particular composition of Na_2O, CaO, P_2O_5, and SiO_2 that enabled it to interact and form strong bonds with the bones and the surrounding soft tissue [21, 22].

The poor survivability of the first generation biomaterials was the main reason behind this development. By mid 1980s bioactive materials had been put to variety of orthopedic and dental applications [10]. Synthetic hydroxyapatite provides a bioactive fixation and was being used on a regular basis as porous implants, powders and coatings for the metallic implants [10].

In Medical surgery one third to half bio-inert and bioactive implants often fail in 10-25 years which results in corrective surgery [23]. The improvements made in the first and second generation biomaterials do not suffice the needs completely, as any man-made implant however efficient; will still lack the ability to receive and response to the stimuli as the living tissue [25]. In order to overcome this issue, third generation of bioactive materials was synthesized. Biomaterials of this generation are being made resorbable and the polymers used are made bioactive. The macoporous foams and bioactive glasses have been designed to activate genes that stimulate regeneration of the tissue [24]. The bioactive glasses used in third generation facilitate the tissue regeneration by supporting osteoconduction and osteoproduction [26].

Forming a composition of biomaterial that has similar biomechanical properties to bones and has sufficient bioactivity to bind to the bone and the surrounding tissue has been one of the toughest challenges in regenerative medicine field [27].

We hypothesize that optimal thermal treatments will show improvement in mechanical properties and biological response of Bioglass 3MVIOX-V3057 similar to the native bone. The optimal sintering treatment will improve the mechanical properties such as compressive strength and density similar to the native cortical bone and biological responses similar to natural human trabecular bone.

Chapter 2: Literature Review

2.1 Bone Morphology and Physiology

The skeletal system that supports entire structure and functionality of the body is an incredible system that has evolved to be as strong as cast iron yet as light weight as wood [28, 32]. It serves the most important function of protecting the delicate organs and is a reservoir of calcium and phosphorus [29]. This is possible due to the structure of bone that contains both flexible and rigid components. The flexible part of the bone is made up of mainly collagen, proteoglycans and number of other proteins. Inside this matrix, rigid component, bone mineral mostly hydroxyapatite is deposited [30].

Broadly, bones can be classified into two types.

1) The cortical (compact) bones: constitute of almost about 80% of the skeleton. They are also found in shafts of the long bones such as femur, tibia, radius, and on the outer surfaces of the flat bones [30].

2) The trabecular (cancellous) bones: make up rest of the skeletal system. They are mainly found at the end of long bones and at the inner portions of the flat bones [30].

Some other components that are part of the skeletal system, Periosteum: is the outer membrane of the bones, except the long bones. Endosteum: lines the inner surface of the bones. Osteocytes: are the star shaped cells that are most commonly found in the mature bones. Harvesian canals: are the tubes that are found around the lamellae of bone along the axis.

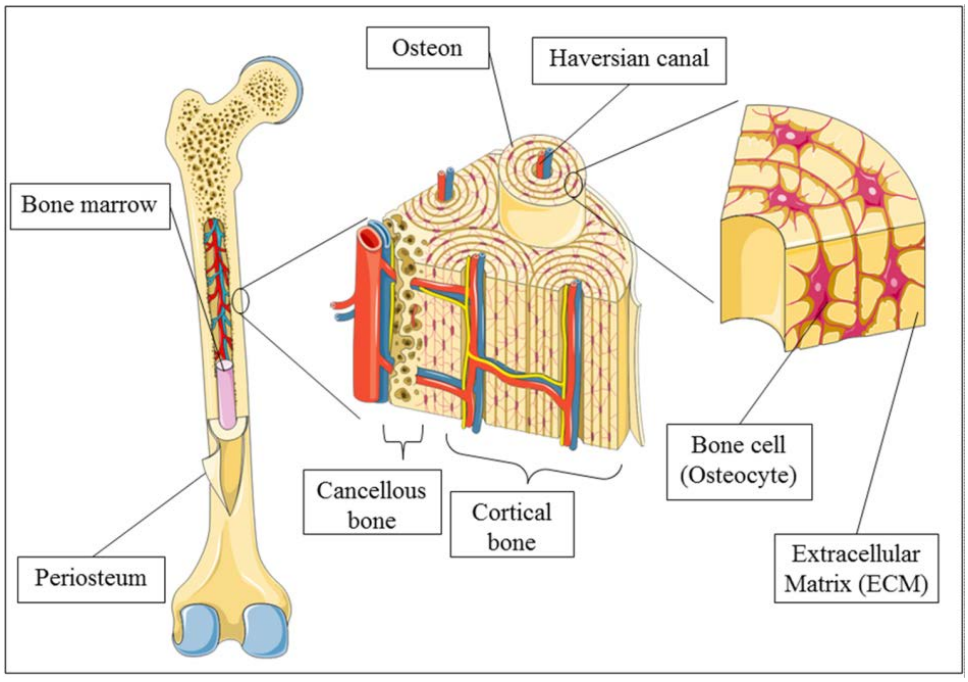

Figure 2.1: Hierarchical Structure of bone [31]

2.2 Bone Development and Formation

Bone like all the other living tissues grows and develops throughout human life. Bone development starts in the 10-13th week of the pregnancy [33]. The process of formation of the bones is called as "osteogenesis". The process starts by

formation of vertebra in the fetus. The skeleton is of the mesodermal origin, and is usually divided in two parts:

1) Trunk (axial) skeleton: comprises of vertebral column, skull, ribs, and sternum.
2) Appendicular skeleton: that consists of limbs [33, 34].

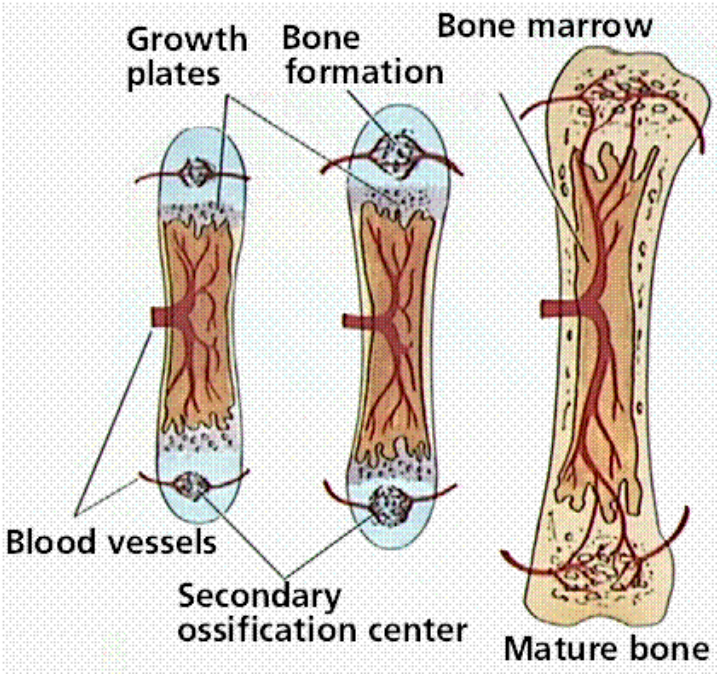

Figure 2.2: Bone growth initiating at the growth plates and resulting in a mature bone [35, 43].

The skeletal system grows throughout the life by process called as, ”ossification”, (Fig 2.2) which refers to formation of new bone over the old bone tissue. Bones also get modeled and remodeled throughout. The process of modeling of bones refers to change in overall shape of the bones in response to the physiologic influence or mechanical forces. Modeling may lead to a gradual change

in the skeleton to the adjustment to the forces that it faces [32, 36]. Modeling may be increased because of hyperthyroidism [37], renal osteodystrophy [38], or treatment with anabolic agents [39].

Bone remodeling is the method in which bones are renewed to increase the strength and mineral homeostasis. In this process, parts of the old bones are continuously removed and are replaced with the new tissue. Remodeling is observed in adults more often than modeling of bones [40]. There is a tightly coupled complex of osteoclasts and osteoblasts that work together in remodeling. Osteoclasts help in resorption of the old bone tissue [41] and osteoblasts help in formation of the new bone that replaces the old bone tissue [42].

2.3 Bone Natural Growth Factors

Growth factors are the substances or proteins are required for stimulation of cell growth. Some of the factors that initiate bone growth are, bone morphogenetic proteins (BMP), transforming growth factor β (TGF-β), Insulin like growth factors I and II (IGF I and II), platelet derived growth factor (PDGF), basic and acidic fibroblast growth factor (bFGF and aFGF) [44].

Each of these factors has a family of genes that are activated in different scenarios and that facilitate cell proliferation and cell differentiation [45]. TGF-β and BMPs 2-7 are subfamilies of the TGF-β family. IGFs, TGF-β and BMPs are made and secreted by osteoblasts. *In-vivo* studies show that these factors

increase the bone formation systemically, promote fracture healing and increase the growth of living tissue around the implants [45]. Out of all the growth factors BMPs have been extensively studied. BMPs are potent osteoinductive factors. They induce mitogenesis in the mesenchymal stem cells and other osteoprogenitors and their differentiation towards osteoblasts [46].

The bone scaffolds and bone substitutes that were used previously do not have the properties for osteoconductive or osteogenic [47]. The deminerialized bone matrix and collagen are the materials used in bone graft extension, but these materials provide minimum structural support to the bone [47]. HA, β-TCP and calcium-phosphate cements, and glass ceramics are used as adjuncts or alternative to autologous bone grafts [48]. They promote proliferation and differentiation of bone cells for bone regeneration. Now a day's bioactive glasses that are used as scaffolds in tissue engineering are the most compatible with the tissue and have similar mechanical properties of the cortical bone.

2.4 Mechanical Properties of Bones

Different types of bones play different roles in human body. These roles depend on their mechanical properties and cell composition. In the previous part we took a look at what the bones are made up of and how they develop. Now we will go through their mechanical properties. As mentioned in the introduction, bones are classified into two types.

Cancellous or trabecular bones: Cancellous bones are porous and have many applications because of their energy absorption capabilities. Due to their porous nature they help in transmitting and distributing the stresses, particularly in vertebral column, in synovial joints, and near ligamentous and tendinous attachments [43-45]. The stress-strain curve reveals the materials' tensile strength and other data that are required to calculate modulus of Elasticity. The stress-strain curve rigid plastic material and cancellous bone are almost the same, as shown in Fig 2.3 and Fig 2.4 the stress-strain curve follow the almost same trend [49]. The curve starts with an initial linear region followed by yield. After the yield point we can see a long plateau where the stress remains constant even when strain is changed. When strain is extremely high the pores start getting filled by debris and become rigid. This long plateau region represents higher capacity of energy absorption.

In a study done on cancellous bones, the correlation coefficient between compressive strength and apparent density was found to be 0.7 which is enough to deduce that as the apparent density increases compressive strength of the cancellous bone increases [50]. Similar phenomenon is observed in the bioactive glasses which will be discussed in later parts of thesis. Compressive strength of cancellous bones is mostly affected by aging. It is found maximum in the young adults and goes on decreasing as the age increases [50].

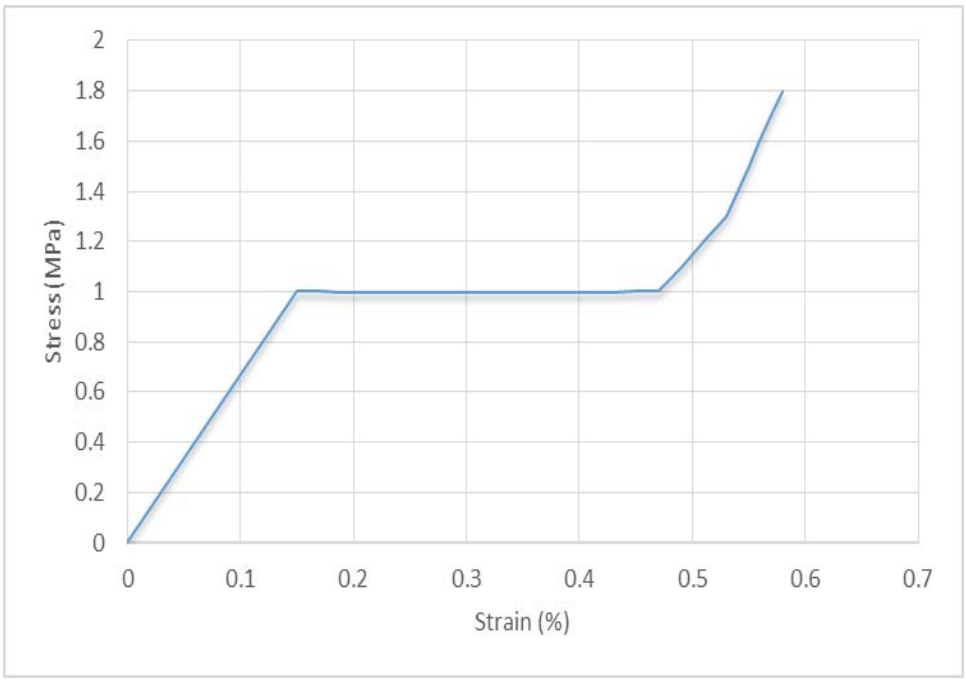

Figure 2.3: The strain-stress curve of the rigid plastic material, apparent density 0.2 gm/cm^3 [49].

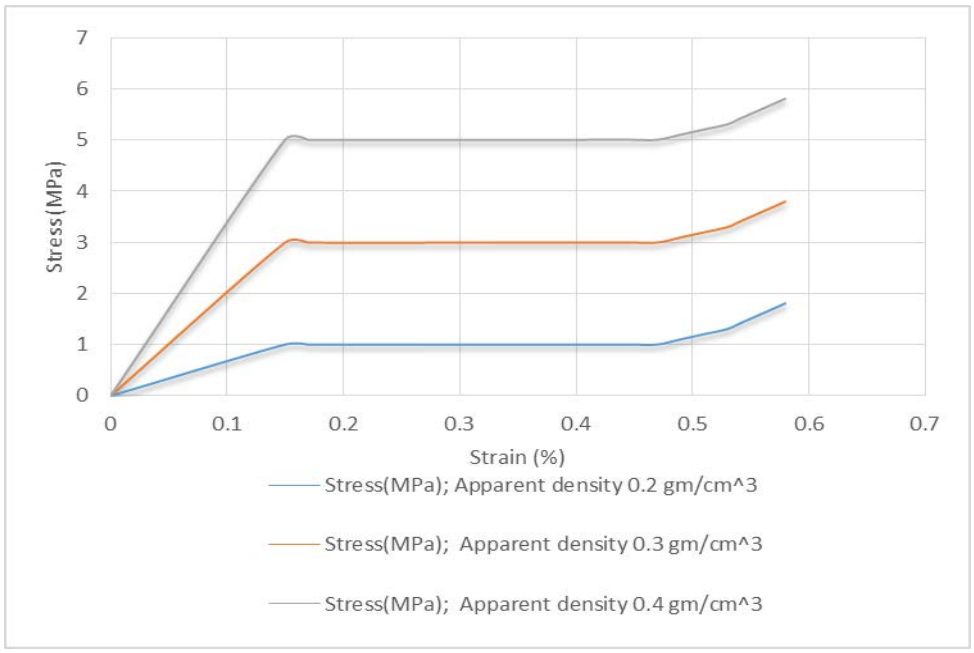

Figure 2.4: The stress-strain relationship of the cancellous bone at different densities [49].

Cortical bones are important because they make up about 80% of the skeletal system. They are found in shafts of long bones such as femur, tibia, and radius. They are also found on the outer surfaces of the flat bones [30]. They are stronger and stiffer than cancellous bones in both longitudinal and transverse direction. The mechanical properties are anisotropic [50]. The compression strength is higher than the tensile strength [50]. Cortical bones display linear elastic behavior. From a qualitative purpose, they break at relatively low values of strains after a marked yield point. Yield point was set by 0.2% offset techniques. This does not reflect plasticity [51].

Creep is the phenomenon of gradual change of the material that may or may not lead to permanent deformation. Creep response of the cortical bone was recorded for different values of stresses. When the stress is low, strain remains constant for most of the time and the bones do not show permanent deformation after unloading. For the values of stresses just above the yield point, strains remain same but there is a small amount of permanent deformation observed. The stress values well above the yield point creep increases and results in lot more permanent deformation [51]. The strength of these bones changes with age. There are data that show 2% decrease in tensile ultimate strength of cortical bones per decade [52, 54]. With this in mind it is intuitive that the energy required to fracture the bone per area is much less in the older bone than in the younger bone [53].

Chapter 3:

Bioactive Glasses in Tissue Regeneration and Regenerative Medicine

Musculoskeletal diseases and deformities are one of the most common medical conditions globally. It results in a substantial impact on health and quality of life. The corrective surgeries are difficult in case of the large bones. It requires lot of time for healing and there is always risk of rejection and scarring [55].

Initially the grafts from a donor were used, known as allograft, but that would often result in rejection by the recipient. To overcome rejection of the allograft, grafts from the patient itself, known as autograft, were widely used. Autograft has a problem of its own, it needs a second incision site which increases scaring and risk of infection [56]. To eliminate the need of grafts from other donor or self, biomaterials have been used for a long time now to replace the damaged or diseased tissue or organ. The controlled microenvironment and proper scaffolding of the bioactive glasses has now led to regeneration of the tissue or organ [10]. Bioactive glasses are the most compatible and pose lesser risk to the patient, they heal faster and they also initiate bone regeneration which is definitely favorable.

The bioactive glasses with P_2O_5-Na_2O-CaO-SiO_2 in them form crystals when given a sintering. Mechanical strength of the material basically depends on crystallized volume fraction and crystal size. Variation in the sintering treatment results in different crystallized volume fraction and crystal size. Carefully

controlled sintering process optimum crystallized volume fraction and crystal size that results in increased tensile strength of the bioglass having same composition [51]. Crystallization also changes with the sintering treatment and the composition used in the process. Two different compositions were exposed to thermal treatment and simulated body fluid solution (SBF-K9). Increased crystalline% resulted in slower formation of HCA layer, but was not inhibited, which shows biological activity of the bioactive glasses. The rate of development of the HCA layer is much higher *in vitro* in these compositions than in commercially available biomaterials like synthetic hydroxyapatite ceramic, A/W glass ceramic, and other third generation bio-ceramics [58].

3.1 Chemical Composition of Third Generation of Bio ceramics: Bioactive Glass

The chemical composition of the bioactive glass plays a major role in its mechanical properties. Major component of the bioactive glasses is pure silica, followed by calcium carbonate, sodium carbonate, and sodium phosphate. Two compositions used in my study are: 1.07N2C3S and $1.5Na_2O$-1.5CaO-$3SiO_2$ with varying percentages of P_2O_5 (0, 1, 2, 4, and 6 wt %) [57]. Biological activity of the materials synthesized from the compositions is tested when they are implanted in the body. The activity is function of dissolution of ions that stimulates proliferation and regeneration of the tissue around the implant [10]. The rate of dissolution of the ions has to be optimum in order to be realistic. If the rate of dissolution is extremely high or extremely low they would not be effective.

There are studies that show that the bone regeneration and proliferation of bones takes place at a significantly greater rate in presence of bioactive glasses than presence of synthetic hydroxyapatite [58]. These differences suggest that there are two classes of bioactivities, Class A and Class B [18]. Class A bioactivity leads to both osteoconduction and osteoproduction. This is due to the rapid ion dissolution properties of the material [18, 60]. Class B bioactivity leads to only osteoconduction, due to slower rates of ion dissolution, slower surface reaction, minimal ionic release, and extracellular interactions take place only at surface [18, 58].

3.2 Third Generation of Bio ceramics: Scaffold for Bone Regeneration

There are three methods that are used for manufacturing scaffolds. The most common one used is the formation of glass from melt-derived glass particle. These melt-derived glass particles are then constructed into the architecture that is desired. The construct is then sintered and made strong enough for the implantation [60]. The other, less frequently used method is called sol-gel processing of the solution having desired components. Recently, new method of electro spinning of the solution into pliable scaffolds containing nano materials is being used [60].

Melt derived glass particles can be formed via process of thermal bonding of the scaffolds. Pore size, porosity and pore interconnectivity are

important properties of the bioactive scaffolds. These properties can be altered using different temperatures and changing the time of exposure [61]. Another method of scaffold building is mixing the desired composition with a fugitive stage solution (like NaCl or an organic solution such as starch); this solution is later removed using dissolution [60, 61]. Polymer free form replication is also a technique used in making scaffolds [60]. This technique gives the most similar to the human bone microstructure to the scaffold.

Polymer free form replication gives the highest porosity. This porosity is similar to the trabecular bones [62]. Another method that is becoming popular is solid freeform fabrication. This method gives the most similar porosity and pore size. The SFF method includes designing the scaffold on the computer using computer aided designing software [63].

The less commonly used method is sol-gel processing method. In this method, solution is foamed using a surfactant. The foaming is followed by condensation and gelation reactions. This gives the structure similar to the trabecular bones of humans. The hierarchical pore size is beneficial in creating a physiological environment [60, 64]. Nanopores initiate better interaction with the tissue and faster HCA layer growth but they are not as strong as the melt-derived scaffolds [60, 65]. The recent technique uses electro spinning to create nonfibrous scaffolds. The goal of these scaffolds is to form a matrix of scaffold that resembles the extra cellular matrix structurally [66, 67]. The material formed using this electro spinning is later subjected to sol-gel process with an inorganic/organic solution. It

is then subjected to sintering [60]. The material formed after the heat exposure is very pliable and it has a higher degradation rate owing to the fine fiber diameter. This has potential applications in the regeneration of non-loaded bone and defects that include the healing of soft tissue.

3.3 Tissues-Surface Interaction of Bioactive Glasses

The physical and chemical reactions that are involved in the implant-tissue bond formation are very well established now. These reactions are known as surface reactions [59]. Transition temperature of the material is defined as, "the range of transformation when the amorphous substance is changed into a super cooled liquid on heating" [68]. Many properties of the material depend on the transition temperature, one of them is crystallization. Crystallization will resist the ion exchange between the implant the aqueous phase which will slow down the initial interactions. There are 11 classified steps in surface reactions [68]. It begins with formation of SiOH bonds, followed by polycondensation of the SiOH leading to form Si-O-Si. Next step is adsorption of amorphous $Ca+PO_4+CO_3$; this is followed by formation of Hydroxyl Carbonate Apatite (HCA layer) [60, 72].

The detailed reactions take place in following manner:

First stage involves rapid dissolution Na^+ and K^+ with H^+ or H_3O^+, this interaction results in formation of SiOH (Silanols) at the interface. Condensation and repolymerisation of SiO_2 rich layer takes place giving result to -

Si-O-Si-O-Si-O. This step is followed by migration of Ca^{2+} and PO_4^{3-} groups to the SiO_2 rich layer forming Cao-P_2O_5 rich film. This amorphous layer increases in size by dissolving more Ca^{2+} and PO_4^{3} ions.

The next step in surface reactions is crystallization of Cao-P_2O_5 film. This takes place by incorporation of the OH, or CO_3^{2-} or F ions, results in mixture of hydroxyl carbonated apatite (HCA) layer and hydroxyl fluorapatite (HCFA) layer[59, 68 and 72]. These are the reactions that take place between the implant itself. Hereafter, the reactions taking place involve the surrounding tissue. The involvement of tissue is what makes the bioactive glasses a huge success in tissue engineering and regenerative medicine The next step involves adsorption of biological moieties in the HCA layer. This step is followed by action of macrophages, attachment of osteoblasts stem cells, differentiation and proliferation of the osteoblasts, generation of matrix, and last by crystallization of matrix and growth of bone [60, 61].

3.4 Mechanical Properties of Bioactive Glasses

As in the living tissue, mechanical properties of the bioactive glasses also depend on the composition and the treatment that the materials are subjected to. Mechanical properties can be altered depending on what the implant is required for [68]. When bioactive glass is made, there is crystallization in the material. Crystallization increases the mechanical strength to a greater extent [57]. The

mechanical strength of the bioactive glasses is representation of its density, and its compressive strength.

Compressive strength of any biomaterial is defined as the maximum stress a material can sustain under crush loading. The compressive strength of a material that shatters in compression can be defined fairly within the narrow limits as an independent property. However, if the compressive strength of materials does not shatter in compression needs to be defined as the amount of stress required to distort the material an arbitrary amount. Information about stress and deformation of materials under uniaxial compressive stresses is obtained from the compression test. To effectively evaluate any non linear stress behavior which may develop as result of cumulative damage process, uniform stress states are required. Maximum load when divided by the original cross-sectional area gives the compressive strength.

A study was done to investigate and compare the *in-vivo* response of the biosilicates to the response given by bioglasses [69]. Biosilicates with composition P_2O_5 - Na_2O-CaO-SiO_2 was implanted in rats with tibial defects. 20 days after implanting three point bending test was performed. This test revealed a higher maximum load failure and stiffness in borosilicate group. These values were similar to the uninjured bones [69]. Biosilicate also showed more bone resorption. This study reveals that fully crystallized biosilicate has good bone forming and bonding properties [69].

3.5 Factors Affecting Mechanical Strength of Bio ceramics

Mechanical strength of the bioactive glasses is affected by many factors such as porosity, grain size, temperature, inclusions, and compressive layers. Porosity is defined as the pore size of the bioactive material. Density and porosity are inversely proportional to each other. The strength of material has a direct relation with density, so as porosity increases, density and strength of the material decreases. Optimum porosity is important because porosity helps the implant-tissue binding by facilitating ion exchange [70].

Pore size, number of pores and shape of the pores present have a combined effect on the strength of the material [70]. Grain size is the next factor that affects the strength of the material. Strength of material follows a direct relation with inverse root of grain size ($G^{-1/2}$), but that does not mean that the strength keeps increasing as the grain size decreases. For very fine particles, grain size almost has no effect on the strength [70]. Temperature plays very important role in strength of the material. The biomaterials when subjected to high temperatures undergo crystallization depending on the percentage composition. As seen before crystallization increases the mechanical strength to a greater extent [57, 62, and 70]. Addition of a compressive surface layer usually results in increased material strength [70]. This layer makes sure that stress that is faced by the implant is divided in an even way.

Chapter 4: Dr. Oonishi's Experiment

The three types of implant that are used in corrective surgeries of orthopedic system in human beings are bioinert implants, bioresorbable implants, and bioactive glasses. Bioinert materials are mostly used in the cases where the tissue is damaged beyond repair. Bioresorbable materials are used where there is chance to repair or regrowth of the tissue [71]. Both these types of implants served their purpose, but they had increased risk of infection, longer healing time and a lesser functionality of the tissue. Bioactive glasses were designed with better solution for the problems mentioned above.

Dr. Oonishi and his colleagues performed a study on three types of implant materials. [72, 73] For testing the biological interactions of these implants, they damaged the tibular bones of rabbits. Three 6 mm holes were in the bones. These holes were filled with one type of the material respectively. Then scanning electron microscopic images were taken by euthanizing animals after 2, 3, and 5 days and 1, 2, 3, 6, 12, and 24 weeks [73].

Alumina, Synthetic hydroxyapatite were prepared by sintering at 1200°C in air as described previously, then was crushed into granules and was sieved to produce particles l00–300 μm in diameter and bioactive glass, 45S5 Bioglass, of the following composition (45% SiO2, 24.5% Na2O, 24.5% CaO, 6% P2O5, all in wt %) was prepared by melting reagent-grade chemicals at

1325°C in a covered platinum rhodium crucible, homogenized for 24 h, cast, crushed, and sieved to l00- to 300 μm particles [74].

Apatite-wollastonite glass-ceramic porous granules were made by first mixing glass powder with a foaming agent together at a fixed ratio and the mixture was added into the blocks. Next, the blocks were heated at a high temperature to allow pores to form when the foaming agent was vaporized. This process induced the precipitation of apatite and β-wollastonite crystals. Afterward, the blocks were crushed and the resulting particles were sieved to obtain particles of l00–300 μm.

4.1 Surface Bio Active Ceramics

When HAp granules of 100–300 μm in diameter were implanted, no osteogenesis was seen when spaces of more than 100 μm were left between Hydroxyapatite (HAp) granules and surrounding bone as shown in figure 4.1. There was no binding of HAp to bone. In the spaces with <20 μm binding of HAp to bone was definitely seen. To achieve sound binding of HAp and bone, the contact area should be extensive [75].

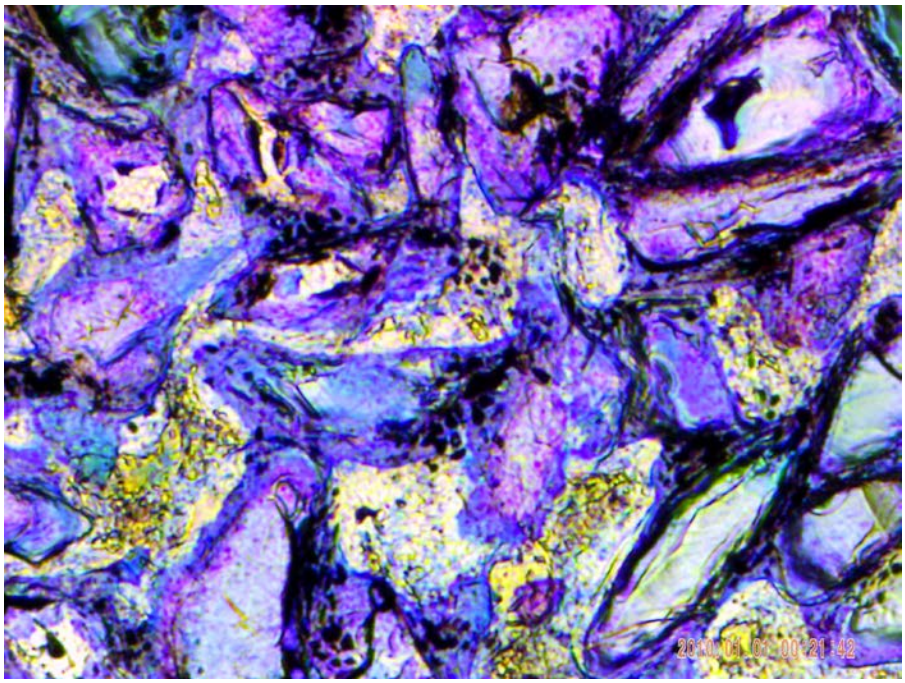

Figure 4.1: Bone growth on HAp (100–300 μm) at 6 weeks. [Adopted 75]

Firm fixation is also important to establish secure contact between bone and HAp. When implanting HAp into the bone, it is important to pack HAp granules firmly into the bone. New bone tissue would not enter spaces between HAp granules which were separated by more than 100 mm. Between 20 and 100 mm, large portions were not filled by bone tissues, but spaces <20 mm were almost always filled with new bone. When the gap between the granules is more, the bone formation is less. So in order to get more bone regeneration, the packing of the implant should be done with no gaps.

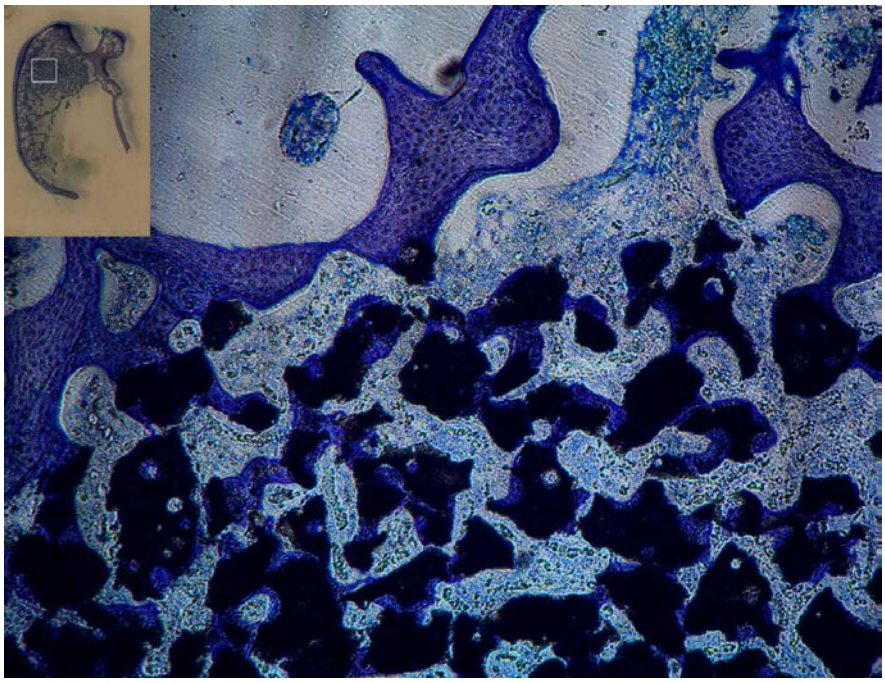

Figure 4.2: Bone Regeneration Healing procedure at 6 weeks with HAp in the trabecular bone. Reference: Dr. Wu and Rajan Pandya

When HAp granules of 10 mm were packed into bone, they were incorporated by 3 weeks but were lost from the trabecular by 6 weeks as shown in figure 4.2 and 4.3. Hence, particular care should be taken to avoid crushing the granules into fine powders whenever HAp granules are packed or driven into bone for clinical use [72].

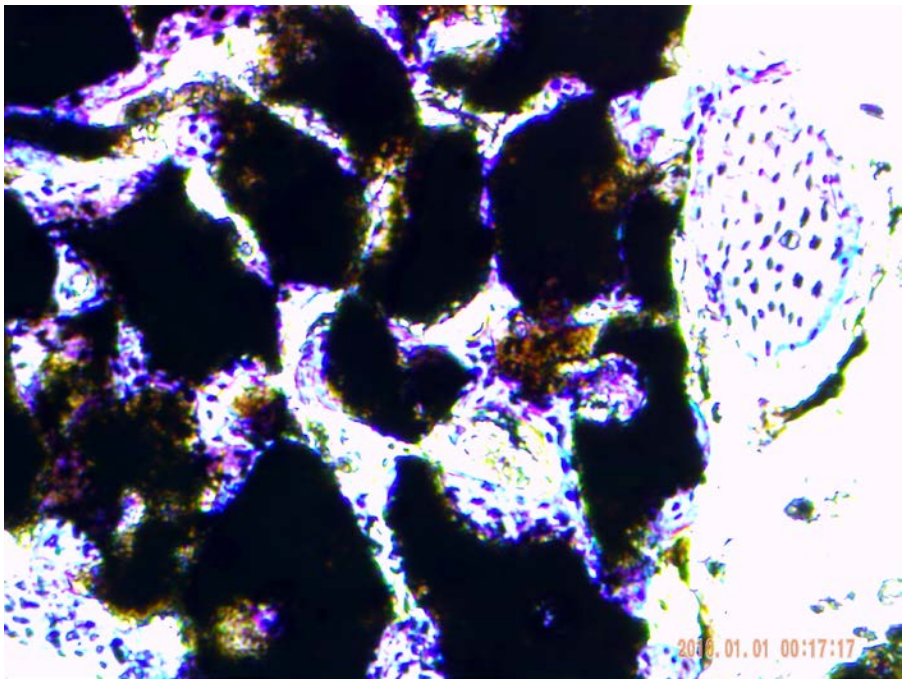

Figure 4.3: Growth on HAp (1–3 μm) at 3 weeks.[Adopted 75]

The experiments showed maximum bone regeneration in bioactive glasses and resorbable material, Tri-calcium phosphate (TCP) as shown in figure 4.4 and figure 4.5. The trabecular contain small numbers of particles. The bioinert implant did not show any bone growth in any particle size or time period.

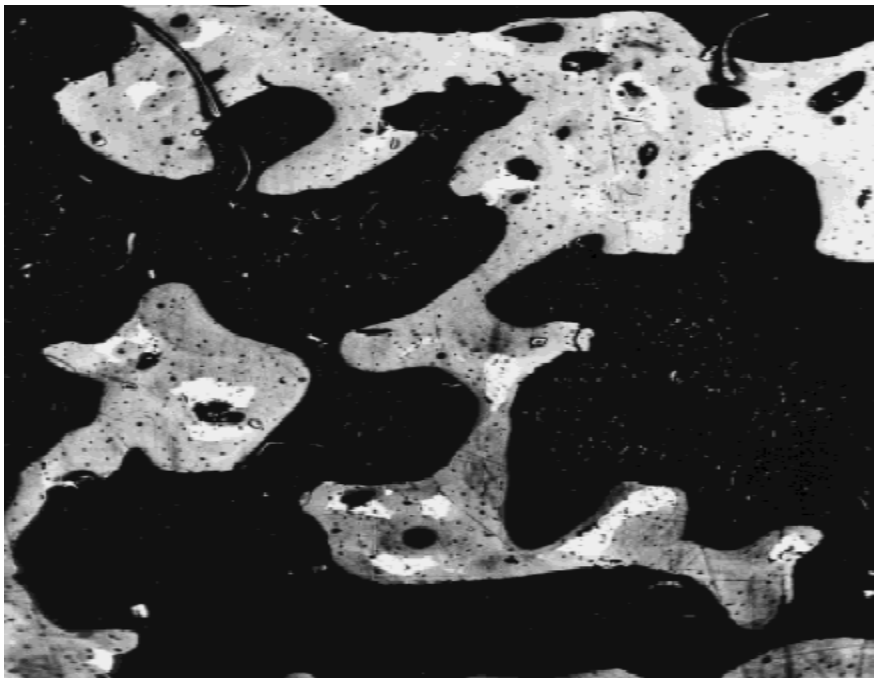

Figure 4.4: Bone growth on a-TCP (100–300 μm) at 12 weeks.[75]

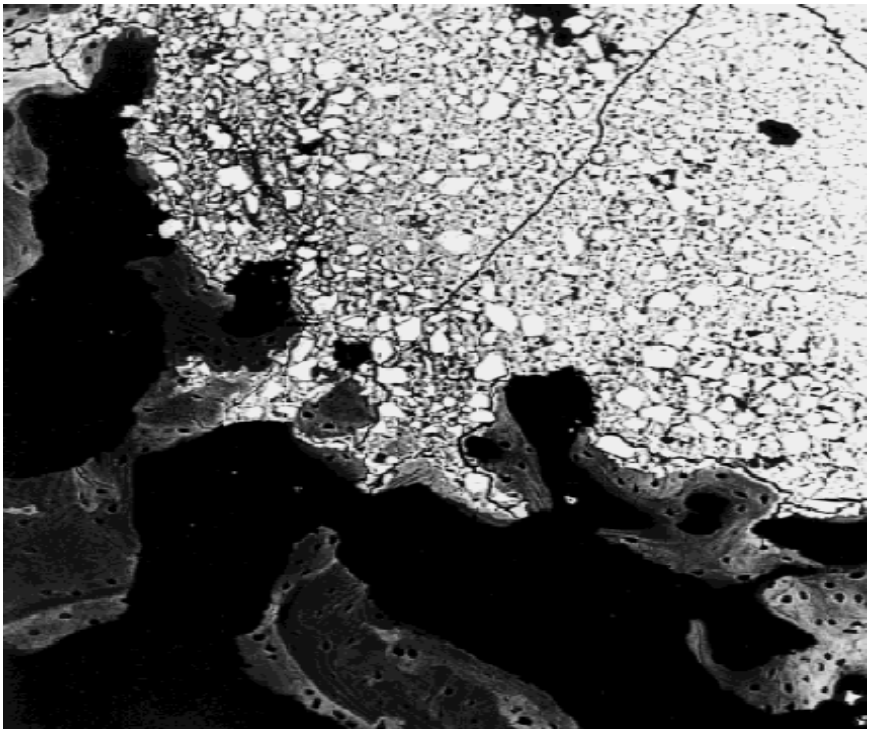

Figure 4.5: Bone growth on a-TCP (10 μm) at 3 weeks [75]

4.2 Bone Regeneration: Third generation bioactive materials

The zone of very fine granules around the bioglass particles was seen around every particle till the center of the defect. Regenerated bone was found on the surface of the bioglass particles till the center. Inter-particle spaces of both were filled by new bone trabecular to the structure as shown in figure 4.6. The amount of new bone in the inter-particle spaces of each type of particle increased [71].

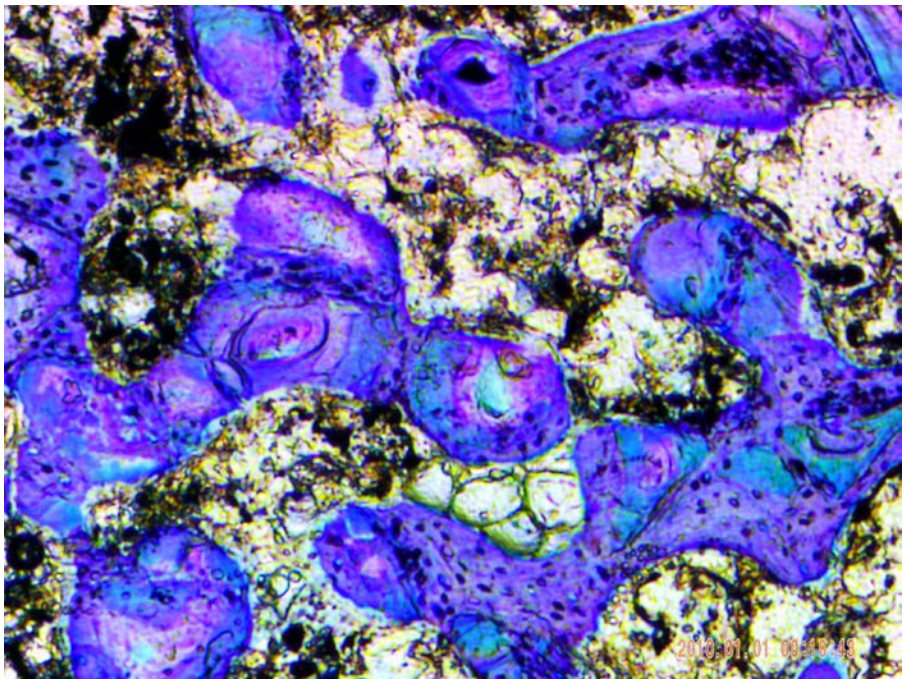

Figure 4.6: Bone growth on bioactive glasses (10 μm) at 12 weeks [Adopted 75]

Chapter 5: Experimental Methods

5.1 Preparation of Bioactive Glasses

Bioactive glasses are scaffold materials for commonly used for bone repair. They are most widely used because of their ability to enhance bone formation and bond to the surrounding tissue. Although brittle, bioactive glass scaffolds provide higher mechanical strength. The silicate based bioactive glass designated 45S5 approved for *in vivo* use [60]. Sintering of 45S5 particles into automatically relevant shapes requires temperature of ~1100ºC or higher. The high temperature leads to devitrification which is process of formation of a predominantly combined crystalline phase. Devitrification makes it difficult to pull the 45S5 glass into fibers.

The composition of "3M-Viox 3057" bioactive glass was used in this experiment. The materials were ordered by Dr. Larry Hench from Ceradyne, inc, Ceradyne, inc is a California based company that manufactures advanced ceramics and components [76]. The glass was prepared by melting a mixture of reagent grades. The water quenched granules were chopped into different sizes. In this experimental method ultra-bone glass composition particles (3M-Viox 3057; Hench et al patent) [76] were ground into smaller particles using a mortar and pestle. The particles were then placed in a copper sieve for one minute to separate them based on their size. The copper sieves used were of Hogentogler & co., Inc [77]. These are ordered from China. The sieves are International Standard Organization

(ISO) The sieve's compartments allowed for the collection of the following particle sizes: >800 μm, 700μm, 650μm, 500μm, 300μm, 250μm, >250μm. Once the particles were ground down to their appropriate size, they were placed in graphite bricks (Figure 6.3).

The graphite bricks were ordered from Haimen Kexing Carbon Co. Ltd. The dimensions of the graphite bricks were standard. The dimensions were length 250 mm, height 124 mm, and width 40 mm. We made 24 holes, 0.5" in diameter and 0.75" deep. The graphite bricks have higher melting point so they can tolerate the sintering temperature. The samples were weighed before and after the placement of the bioactive glass particles to determine the total mass of particles in each bulk sample.

The first two times we exposed the mixture to sintering, they did not form the plates we wanted. The graphite bricks underwent degradation in sintering process. To overcome this problem of graphite bricks were used with graphite fireboard and paper in muffle furnace. The fireboard and the paper for muffle furnace was bought from company Matrix, China ltd. The paper is non-flammable and is made from mixing binder with ceramic fibers. The paper is very smooth, and can be cut into any sizes as per the experiment requirements. Low thermal conductivity, good thermal stability, and good stability in chemistry are some of their features that help resist the degradation.

5.2 Thermal Treatments for Bioactive Glass

Sintering is the process of controlling both densification and grain growth. Bioactive glasses are highly biocompatible and exhibit a strong interfacial bond to bone. Their bioactivity is attributed to the formation on their surface of a hydroxycarbonated apatite (HCA) layer similar to the bone mineral [10]. This diffusion is caused by a gradient of chemical potential. There is movement of atoms from an area of higher chemical potential to an area of lower chemical potential.

A muffle furnace is mostly a front-loading box-type oven or kiln for high temperature applications such as fusing glass, creating enamel coatings, and ceramics. The furnace we used was Thermolyne furnace model FB1415M, which we got from LabX Company. The sintering process of 45S5 Bioglass powder (mean particle size < 5 μm) investigate by using different thermal analysis methods. Using heating microscopy and conventional dilatometer techniques it was found out that there are two major steps in sintering of the bioactive glass: The first stage is called the short stage, the temperature used in this stage ranges from 500–600 °C and in the second stage or also called the longer stage, the temperature range is 850–1100 °C [78]. In this experiment 1100-1200 °C temperature ranged used for proper sintering.

Differential thermal analysis (DTA) technique was used to show that Bioglass® crystallizes at temperatures between 600 and 750 °C for 240, 360, and 600 minutes. Na2Ca2Si3O9 showed the main crystalline phase when the samples

were sintered at 1150°C for 120 minutes. These results can be use for designing the sintering-crystallization heat treatment for Bioglass powder which is used for fabricating tissue engineering scaffolds with varying degree of bioactivity. Sintering is followed by nucleation and crystallization process.

5.3 Mechanical Testing.

Sample preparation was a very simple protocol. 3M-Viox 3057 was taken. The particles at this moment were of uneven sizes. These particles were first ground using mortar and pestle. The ground particles were sieved using copper sieves. This step ensured that the particles obtained were of almost same size. The process of grinding and sieving was repeated many times to get sufficient amount of sample to fill in the graphite bricks.

After the samples were prepared, determination of compressive strength was the next step in the protocol. The compressive strength of the material was determined using stress-strain behavior, under monotonic uniaxial loading of advanced ceramics at ambient temperature. The protocol followed is specific for certain specimen geometries. In addition to the compressive strength, test specimen fabrication methods, testing modes (load or displacement), testing rates (load rate, stress rate, displacement rate, or strain rate), allowable bending, and data collection and reporting procedures are addressed. Compressive strength as used in this test method refers to the compressive strength obtained under monotonic uniaxial

loading. Monotonic loading refers to a test conducted at a constant rate in a continuous fashion, with no reversals from test initiation to final fracture.

Values expressed in this test method are in accordance with the International System of Units (SI) and IEEE/ASTM SI 10 [79].

5.4 Compression Test for Bioactive Glass

Compression test can be used for material development, material comparison, quality assurance, characterization, and design data generation. It also provides information on the strength and deformation of materials under uniaxial compressive stresses. The important factor to effectively evaluate any nonlinear stress-strain behavior which may develop as a result of cumulative damage is uniform stress.

Microcracking which may be influenced by testing mode, testing rate, processing or compositional effects, microstructure, or environmental influences needs to be eliminated. Test environment (vacuum, inert gas, ambient air, and so forth) including moisture content (for example, relative humidity) may also have an influence on the measured compressive strength. Test to evaluate the maximum strength potential of a material can be conducted in inert environments or at sufficiently rapid testing rates, or both, so as to minimize any environmental effects.

The calculation of compressive strength of the material is based on the breaking force and cross sectional area of the uniaxial rod. The formula used is $S_u=P_{max}/A$, where

S_u= Compressive strength, MPa

P_{max}= Maximum force, N, and

A= cross-sectional area, mm^2

Instron is used to evaluate the mechanical properties of the materials. The mechanical properties evaluated using different tests for tension, compression, flexure, fatigue, impact, torsion, and hardness tests. These machines have sensors, which are called transducers. The energy received from the specimen loaded is converted by these transducers into an electrical signal. This electrical signal can be used as an input into the mechanical testing system. There are two transducers in the standard electro-mechanical testing system. One of the transducers measures the distance of the position of the crosshead, the second one is to measure the forces exerted on the specimen. An optical encoder installed on the motor records the movement of the crosshead. There is a strain gauge device, called the load cell, connected to the crosshead and is plugged into a Signal Conditioner Module (SCM) in the frame controller. These transducers are used in determining the mechanical properties of the materials. Using the software, all the values can be controlled.

All the parts of the system are connected to control electronics. They include two boards, digital signal processor board and a load conditioner board. There are also optional boards to control the input/output conditioner board, Strain 1 and Strain 2 conditioner boards, and expansion board. The machine that was in the experiments done in this thesis is Instron E3000-5900.

There are a lot of types of tests that are performed by this machine. Some of them are to calculate tension, relaxation/creep, compression, compression relaxation/creep, flexure, flexure relaxation/creep, peel, tear, and friction, tension test profiler (Cyclic), compression test profiler (Cyclic), metals. Out of these method types, we concentrated on the compression strength of the materials we had synthesized. The parameters used for testing compressive strength are same as to check the tension of the material. Test control is set to preload, precycle upto 2 cycles. The calculations involved in the compressive strengths are absolute peak, local peaks, preset points, user calculations, modulus (9 types), yield, (5 types), break (6 types), slack/compliance, correction, Poisson's ratio, area, reduction, break location, seam slippage.

The software called Bluehill 3®. This software helps the Instron to receive the data and analyze it. There are various adjustments done by the adjustment screws can be controlled in the load frame can be preset in the software and the values including extension, and load that give us useful information about the different mechanical properties of the materials can be calculated. For the software to work, the transducers from load frame must already exist in the

software. The values are calculated using a mathematical expression as described before. This software also allows the users to input the measurements. This gives an opportunity to create virtual values. They can be used in case where there are endless possible measurements. A set of all the suitable parameters such as specimen dimension, shape, and applied load rate are selected for testing the material is called a test method. Bluehill 3® enables the user to edit the previously saved methods or new parameters. All the parameters, including the report and graph set up can be changed. Once the parameters are set to desired values, testing can be started.

Figure 5.1: Compression Test on Instron, Reference: Rajan Pandya

Mechanical properties and behavior, for example, shape and level of the resulting stress-strain curve, compressive strength, induced bending are properties that will be affected by fabrication of test specimen. Fabrication can introduce dimensional variations which may have pronounced effects on these properties. Surface of the specimen were made smooth using the dremel tools. Determination of ultimate strength of the pristine material can be interfered by the machining effects introduced during test specimen preparation. The final compressive fracture of advanced ceramics can be attributed to the interaction of large numbers of micro cracks. These micro cracks are generated in the volume of the material and ultimately lead to loss of structural integrity. We determine that these micro cracks lead to fracture and breaking point is determines maximum compressive strength.

5.5 Bioactivity Test

Most of the biological reagents used in bioactivity testing are hydroscopic, so the containers should be left open for minimum time and resealed with parafilm as soon as the required volumes are taken out. Experiments should be carried out in timely manner to avoid evaporation of the reagents.

The stains used in the bioactivity testing are eosin and methylene blue. Eosin is an acidic stain, which means that it binds to positively charged molecules or bases. Methylene blue is a cationic stain that binds to the negatively charged ions or acids. Eosin binds to positively charged ions that leach out from

samples while the HA layer forms [80]. This is the reason why there is stain bleeding in case of eosin. Methylene blue interacts and binds to the negatively charged surface of the HA layer, this is the reason why there is less stain bleeding in case of methylene blue [81].

Tris buffer saline was prepared at room temperature. This experiment needs around 600 ml of tris buffer saline, which is a buffer solution with 50 mM Tris and 150 mM Nacl in it. Preparation of Tris buffer saline requires controlled atmosphere. In the preparation 3.636g of Tris and 5.256g of Nacl was dissolved in 510.5 ml of distill water. The pH of the buffer was adjusted using 1M HCL. In the end pH of the solution is 7.6. Total 89.6 ml volume of HCL was used in adjusting pH.

In-vivo analyzing of bioactivity requires animal sacrifices, are expensive, and involve ethics. So *in-vitro* was technique of staining by eosin and methylene blue. Cell based techniques involve more complex solutions containing biological moieties such as proteins. This increases complexity of the test. The rate of ionic release and pH increases also depends on dynamic or static method used to stimulate biomaterial reactivity. The Tris buffer saline has pH of 8.1 and can be used to buffer solutions of pH 7.1-9.1. It can be used to detect basic deposition of HA layer on the surface of the bioactive glasses. This is useful because the solution does not have any other ions dissolved in it [82].

All of the laboratory equipment used in this experimental set up is: weighing balance of Mettler Toledo Company. This weighing balance is economy

grade milligram balance, measuring cylinder of capacity of maximum of 220g and minimum capacity of 0.0001g, polypropylene containers with screw caps, orbital shaker of Satori Bio Company, pH strips, filter paper and funnel, drying oven, desiccators. Acetone was used at the end in order to stop the reaction.

In Bioactivity test bioglass particles of size 310 μm, weighing 75mg were stained with Eosin and Methylene blue. In this procedure 5 groups were taken to experiment for 10 minutes, 1 day, 2 days, 3 days and one group as control put in DI water for 0 minutes. Experiment performed in triplicates.

Protocol for performing staining test on 310 μm samples of Bioglass: Samples with 310 μm particle size show the maximum amount of porosity with significant compressive strength. Our goal is to find out how these samples react with biological environment.

5.6 Staining Procedure

First 15 samples were weighed and put in glass vials with labels. Each sample was 75mg. Tris buffer was preheat at 37º C in a water bath. All the samples were labeled according to the 5 groups as mentioned before. In one group DI water was added for 0 minutes. This group is treated as our control group. Control samples were stored in desiccator. Other groups were labeled accordingly; warm Tris buffer saline was added to these groups. Tris buffer saline mimics as biological fluid. Different group samples are put in the orbital shaker at room temperature and the shaker is set at 120 rpm.

To start the staining process 15 bioglass samples were weighed (75mg each) and put in 15 small glass vials. The samples were clearly labeled. Next Tris buffer saline was preheated to 37^0 C. The sample put in DI water was used as control. After that, 5 ml preheat pre-warmed Tris buffer saline was added to all the bioglass samples. After adding pre-warmed Tris buffer saline, samples were put in an incubator shaker with 120rpm at 37^0 C. Then, samples were filtered at end of each designated time point (10 minutes, 1 hour) using funnel and filter paper. Next step was to remove all the absorbed salts by washing the samples with DI water. Before leaving the samples, in an incubator at 37^0 C for drying, acetone was added to the vials to stop the reaction.

All the samples were later divided in two parts. This was done by weighing the dried samples and making exact halves if the weight. The dried and divided samples were added to 96 cell culture disk. Adding the stains to the divided samples was the next step. One part of the sample was stained with eosin and the other one was stained with methylene blue. The stain was left there for 10 minutes. After that 200 µl DI water was added to all the wells to wash the unbound stain. Water was left in the wells for about 1-2 minutes and then all the liquid was pipette out. The samples were washed with water several times to remove all the excess stain. Next, the images of the samples were taken using digital camera. Lastly, the plate containing sample was covered with aluminum foil and stored in the desiccator.

After the reaction was stopped, all the three samples of the group were left in the incubator to dry at room temperature at 37º C for 30 minutes. Dried samples were put in the 96 cell culture disk. Next all the samples were stained with Eosin. The stain was allowed to sit for 10 minutes, the samples were kept as it is and the staining process was observed. 200 µl of DI water was put in each of the wells of 96 cell culture disk for 1-2 minutes. DI water was used to wash stain. All the liquid was pulled out of the well. The same wash was done several times until no stain bleeds out from the samples. Photographs of the stained samples were taken from a digital camera.

Same procedure was repeated for methylene blue. The plates containing samples were covered with aluminum foil and stored in a desiccator. Significant results were found out using the digital images of the stained samples. We checked expression of the stains eosin and methylene blue in the samples. Eosin binds to the cations leaching from the HCA layer show less staining. Methylene blue binds to the negatively charged HCA layer and shows more staining.

Chapter 6: Results and Discussion

The microstructure and mechanical properties of the bioactive glass in this study shows significant improvement in compression test. Density measurement of bioactive glass improved significantly with improvement of the nucleation in the samples. Staining pattern observed in bioactive glasses was similar to the staining pattern in the biological substances.

6.1 Sintering Of Bioactive Glasses

Sintering shows both densification and grain growth. Sintering is performed on the bioactive glasses to increase the mechanical strength of the sample and control the porosity of the sample. First step in the sintering was to optimize the temperature and time of sintering in order to achieve the required porosity and mechanical strength.

Before optimization, all the samples were prepared with temperature range 670^0C to 750^0C. In this procedure all the granules from V3037 samples glass frits weighed approximately 1 to 2 g of glass frit and the granules were placed into a ceramic boat for heat treating. 3 to 5 small piles of glass frit were put in the boat. Distance was maintained between each pile so that they do not flow together. Samples were heated for 10, 20, and 30 minutes.

The materials were inspected for adhesion into a sintered mass that still has a high volume fraction of porosity. The temperatures ranges used were 550^0C, 590^0C, 670^0C, 690^0C, 710^0C, 730^0C, and 850^0C temperatures were used. All of the temperature ranges showed partial sintering in the samples. Muffle furnace was used in this experiment. All the samples came out with low sintering behavior. As you can see in the figure 6.1. A batch of 10 samples was used in the early sintering process to quantify the sintering behavior in the samples with temperature range up to 750^0C. Results from previous experiments show very low sintering behavior with all the temperature ranges.

Figure 6.1: Partial Sintering Behavior of Bioactive glasses

(Temperature Range: 550 ^{0}C -850 ^{0}C; Time 192 minutes Followed by 68 minutes).

Table 6.1: Summary of the sintering behavior of the bioactive glass V3057 samples.

Bioactive Glass Ceramics Form	Temperature	Time	Strength	Sintering	Comments
Powder	810-840^{0}C	40	Low	Yes	Getting sintering but shrinking.
Powder	810-840^{0}C	50	Low	Yes	Getting sintering but shrinking.
Granules (310 µm)	810-840^{0}C	40	Very High	Yes	High sintering and Nucleation
Granules (710 µm)	810-840^{0}C	40	High	Partial	Intermediate Sintering and High Nucleation
Granules (870 µm)	810-840^{0}C	40	High	Partial	Intermediate Sintering and high Nucleation
Granules (310)	770-800^{0}C	30	High	Yes	High sintering and Nucleation
Granules (710)	770-800^{0}C	30	Intermediate	Partial	Intermediate Sintering and High Nucleation
Granules (870 µm)	770-800^{0}C	30	Intermediate	Partial	Intermediate Sintering and high Nucleation
Granules Uneven size	750-790^{0}C	90	High	Partial	High sintering and Nucleation but breaks apart

Granules V3037 were sorted into some particle size range using sieves. Four particle sizes were selected including 250 µm, 310 µm 600 µm and 800 µm. All 15 samples prepared in the furnace and heat treat at 550^0C for 192 minutes followed by 34 minutes at 650^0C (3 samples were removed immediately after nucleation and crystallization process; 3 more at 38 min; 3 more at 43 min, 3 more at 48 min, 3 more at 53 minutes.) This heat treatment showed nucleation and grain growth in small crystals in the macro-porous compacts and thereby increased their strength. This procedure showed partial sintering in the particles. Fig shows partial sintering behavior. Muffle Furnace does not give constant temperature for set value. Example: When you set to 750^0C its goes till 790^0C and get back to 750^0C. So there is a considered window for temperature range.

After trial and error method, the optimum temperature and time for bioactive glass V3057 water quenched samples was found to be 1100^0C and 60 minutes in kiln furnace. Samples prepared with optimum time and temperature shows significant amount of strength with high porosity. Fig 6.2 shows sintering behavior of bioactive glass.

This experiment of bioactive glass with ceramics boats showed significant sintering but with little strength. The main problem with ceramic boat was that the samples were getting stuck to the wall of ceramic boat. The samples could not be taken out from the ceramic boats. Results can be seen in Fig as it was broken in pieces. To overcome this problem graphite cylinder was used. And later on graphite brick was used for the perfect size of bioactive samples.

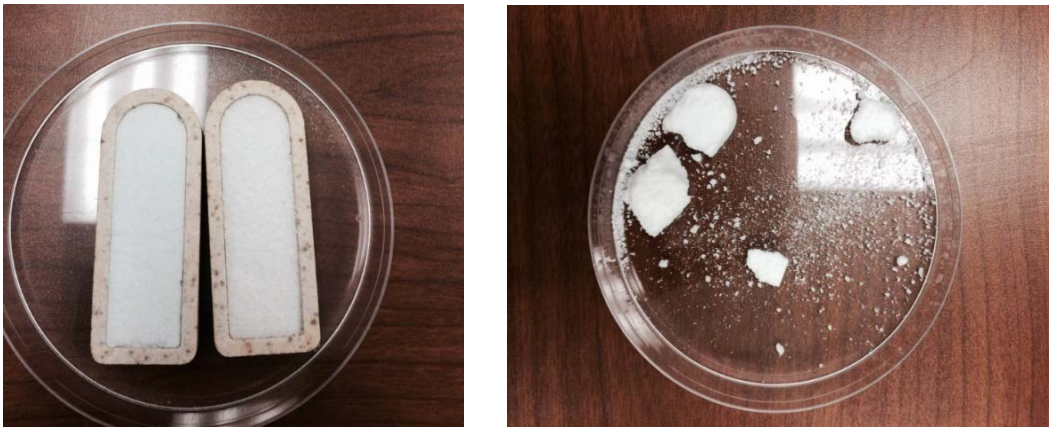

Figure 6.2: Significant Sintering but with low strength Bioactive glass samples.

The first batch of bioactive glass V3057 water quenched prepared in graphite bricks showed perfect sintering behavior with very high strength and also relatively high porosity. Samples came out without sticking to graphite brick's wall. Fig 6.3 shows the significantly improved results of sintering treatment with graphite bricks.

The samples prepared in ceramic boats were stuck to the ceramic boats after sintering. For the further analysis by Instron and SEM, we need smooth surfaces which are obtained by dremel tools. The dremel tools that were used in this experiment were diamond dremel tools of model DREMEL4000. They are also known as rotary tools. To avoid the problem of samples getting stuck to the ceramic boats, we used graphite bricks. The samples did not stick to the walls of graphite bricks and came out as a whole block. Taking out the sample blocks from the samples was also very easy.

Figure 6.3: Perfectly sinter bioactive glass sample; Graphite brick.

All the samples cut in different sizes using dremel tools. The diamond dremel tools help in giving a smooth surface for further analysis to be done by Instron and scanning electron microscope. The cut samples were placed in the ceramic boat and then weighed using the digital weighing balance. The least count of this balance was 0.001 gm. Width, length, and height, were used to calculate the volume of the samples. To measure these values, a digital vernier caliper was used. Figure shows the vernier caliper. The volume calculated from the vernier caliper readings and mass measured by the weighing balance was used to calculate the density of the sample with different sizes was calculated by dividing the volume by mass. Density affects all the other mechanical properties such as modulus of elasticity, and tensile strength of the bioactive glass materials [83].

As we had hypothesized, there is a significant change in the mechanical strength of the bioactive glasses when sintering treatment is changed. This can be seen in the images and the table 1.

6.2 Scanning Electron Microscopy Analysis

Scanning electron microscopy was performed on three samples of each particle size to identify differences in pore sizes and degree of sintering. Once we had the sintered particles, we coated them with gold nanoparticles using Denton Vacuum Desk III sputtercoater. The protocol followed for this process is listed below.

First step in the coating process of the materials was to open the shutter of the coating chamber of sputtercoater. Next, the specimen already on the stub was placed on the stage inside the coating chamber and covered. After covering the coating chamber VACCUM was selected from SYSTEM OPERATIONS drop down menu. Next step was to turn on ROUGH PUMP. Before turning the GAS VALVE from the VACUUM screen, cover of the chamber was pressed down till the pressure began to decrease. The pressure was allowed to come down till 50 mTorr. The pressure at this step should be less. The less the pressure, stability is more. The coating gets better with more stable pressure. After GAS VALVE was turned on, the pressure was allowed to stabilize in between 65-70 mTorr. Before setting sputter time, TIMED SPUTTER was selected from

SYSTEMS OPERATION. Next, the sputter time was turned on. As soon as it was turned on, HiVoltage box was checked immediately, the current was between 20-30 mAmp. The graph on the right hand of the HiVoltage box read below 75%. So the SPUTTER process was left to run for the desired time. After the time got over, the process stopped automatically. Next ROUGH PUMP was turned off by returning to the VACUUM screen. Lastly, cover was opened and specimens were taking out after waiting for about 30 sec.

These particles were later observed using backscattered scanning electron microscopy using JEOL-JSM6380 LV scanning electron microscope. The resolution of the JSM-6380 microscope is 3.0 nm. It is therefore called high performance. It is also low cost equipment, compared to other microscopes with similar features. The machine can be intuitively operated because of the customizable GUI. The software used in this SEM is called Smile Shot™. This software ensures optimum operation settings. The specimen chamber of JSM-6380 can accommodate a specimen of up to 6-inches in diameter. Auto focus/auto stigmator, auto gun (saturation and alignment), and automatic contrast and brightness are some of the standard automated features of this microscope.

Eucentric stage and conical lens are some of the other distinguishing features of JSM-6380. Multiple options that increase versatility give JSM-6380 a broad spectrum of applications. Other highlights of JSM-6380 include: fast, unattended data acquisition (with optional stage automation), smart settings for common samples, streamlined design, compact footprint, customized toolbars for

repetitive functions, enhanced imaging, super conical lens. Images of each sample were taken at 30X, 60X, and 110X magnifications. Images were taken of the top, bottom, and internal surfaces of each sample.

Density and grain size can be controlled by sintering. Diffusion of the atoms through the microstructure leads to sintering. SEM image analysis uses different magnification for quantification of bioactive glass images. Higher magnification shows clear but small amount of sintering between particles.

The small size particles Ultrabone glass 250 μm show good amount of sintering at optimum temperature and the sintering time, which can be analyzed using SEM. The figure 6.6 shows backscattered SEM images of the bottom surface of the sample.

In figure 6.6(A) it can be seen that, the particles of size 250 μm that have been treated at 1000-1020^{0}C. The particles have sintered together in a very less amount because the time of exposure was only 60 minutes. Figure 6.6(B) shows the particles of size 250 μm that were treated at 1000-1020^{0}C. The particles were exposed to the thermal treatment for 60 minutes. These samples were exposed to nucleation and crystallization thermal treatment. The temperature and time exposure used for this thermal treatment was 550^{0}C for 192 minutes, followed by 660^{0}C for 68 minutes. As it can be seen in the figure 6.6(B) there is good amount of sintering between particles.

Figure 6.6(C) shows the particles of size 250 μm that were treated at 1000-1020^{0}C. The time of exposure was increased to 120 minutes. Nucleation and crystallization thermal treatment was applied to these samples. The temperature and time exposure used for this thermal treatment was 550^{0}C for 192 minutes, followed by 660^{0}C for 68 minutes. After this treatment as it can be seen in the figure 6.6(C) there is a little increment in the amount of sintering between particles than the previous treatment. Figure 6.6(D) shows the particles of size 250 μm that were treated at 1100^{0}C. The particles were exposed to the thermal treatment for 120 minutes. These samples were then exposed to nucleation and crystallization thermal treatment. The temperature and time exposure used for this thermal treatment was 550^{0}C for 192 minutes, followed by 660^{0}C for 68 minutes. Particles shown in the figure 6.6(D) show very good sintering, but the porosity of the samples is lost to a greater extent making it less compatible with the fracture site.

The small size particles Ultrabone glass 250 μm show good amount of sintering at optimum temperature and the sintering time, which can be analyzed using SEM. The figure 6.7 shows backscattered SEM images of the internal layer of the sample.

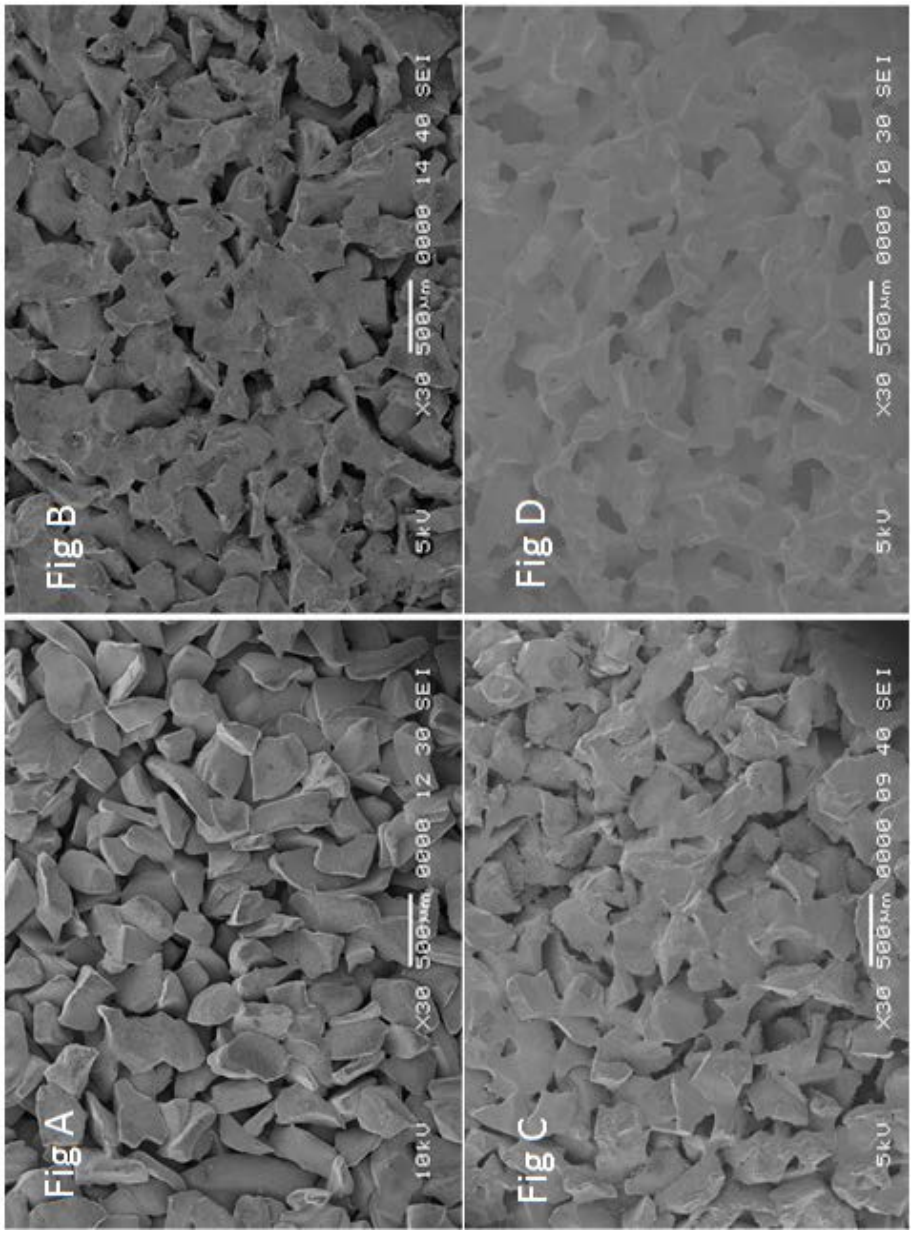

Figure: 6.6 SEM Back scatter bottom surface images for 250 µm particle size

In figure 6.7(A) we can see, the particles of size 250 µm that have been treated at 1000-1020^{0}C. The exposure time for these samples was 60 minutes. The particles, as seen in the diagram, did not sinter together at all. Figure 6.7(B)

shows the particles of size 250 μm that were treated at 1000-1020^{0}C. The particles were exposed to the thermal treatment for 60 minutes. These samples were exposed to nucleation and crystallization thermal treatment. The temperature and time exposure used for this thermal treatment was 550^{0}C for 192 minutes, followed by 660^{0}C for 68 minutes. Even after applying the crystallization and nucleation thermal treatment to the samples, there was no sintering observed.

In figure 6.7(C) we can see the particles of size 250 μm that were treated at 1000-1020^{0}C. The time of exposure was increased to 120 minutes. Nucleation and crystallization thermal treatment was applied to these samples. The temperature and time exposure used for this thermal treatment was 550^{0}C for 192 minutes, followed by 660^{0}C for 68 minutes. After this treatment as it can be seen in the figure 6.7(C), there is little amount of sintering in the internal layer of the sample, which shows sintering goes to internal layers with increase in temperature and time of exposure.

Figure 6.7(D) shows the particles of size 250 μm that were treated at 1100^{0}C. The particles were exposed to the thermal treatment for 120 minutes. These samples were then exposed to nucleation and crystallization thermal treatment. The temperature and time exposure used for this thermal treatment was 550^{0}C for 192 minutes, followed by 660^{0}C for 68 minutes. Figure 6.7(D) is used to compare the amount of the sintering in the other samples. The internal layers show lesser amount of sintering than the outer surface of the sample. Sintering behavior of the sample decreases as we go towards the inner surface of the sample. This

behavior is similar in the cortical bone; this was shown in Dr. Oonishi's paper. The bone regeneration of the bone is the maximum on the outer surface of the bone [75].

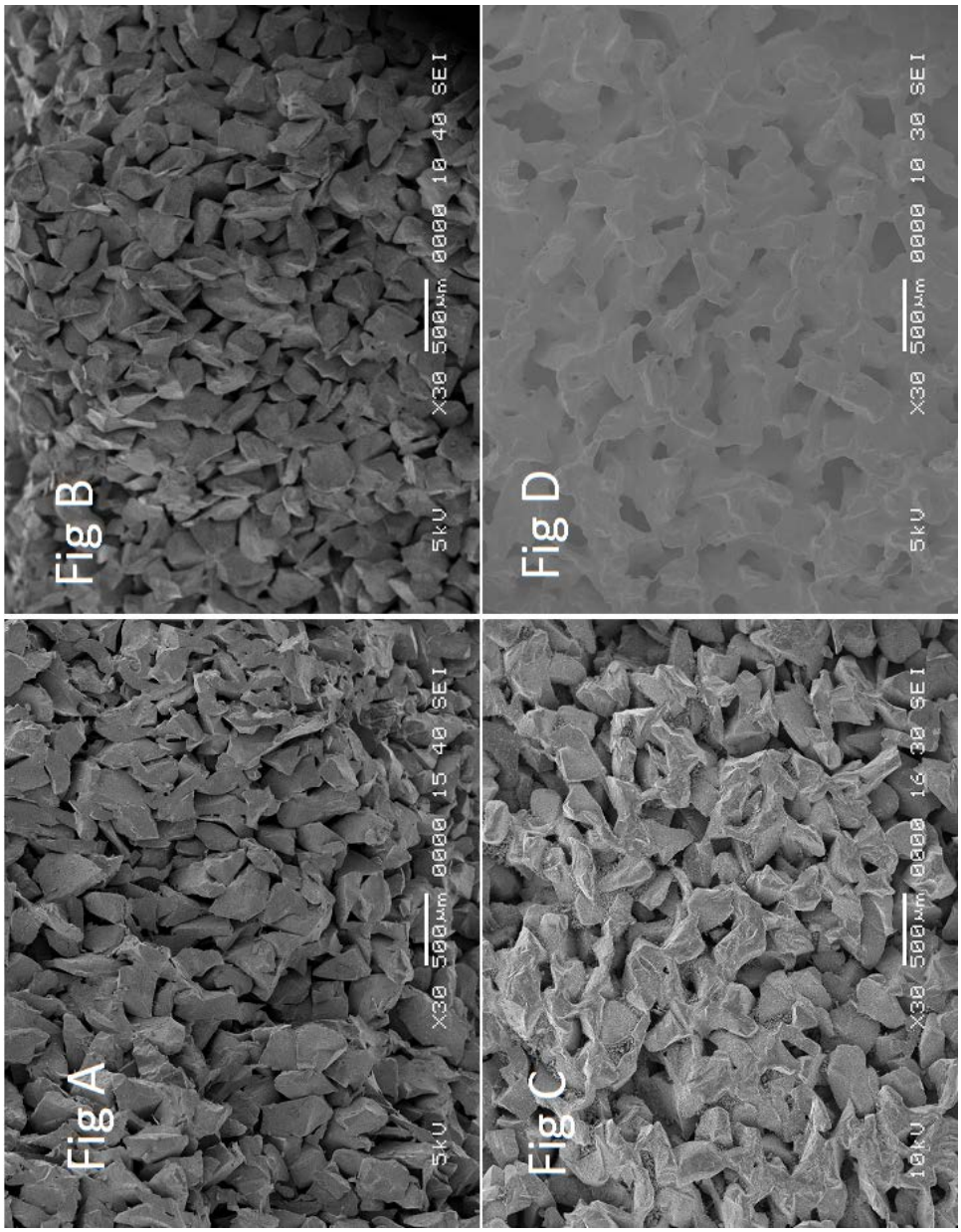

Figure: 6.7 SEM Back scatter internal images for 250 µm particle size

The size particles Ultrabone glass 310 μm were subjected different sintering temperatures. The figure 6.8 shows backscattered SEM images of the bottom surface of the sample.

Figure 6.8(A) shows the particles of size 310 μm that have been treated at 1000-1020^{0}C. There is very little amount of sintering is seen in these samples because the time of exposure was only 60 minutes. In the figure 6.8(B) we can see the particles of size 310 μm that were treated at 1000-1020^{0}C. The particles were exposed to the sintering thermal treatment for 60 minutes. These samples were exposed to nucleation and crystallization thermal treatment. The temperature and time exposure used for this thermal treatment was 550^{0}C for 192 minutes, followed by 660^{0}C for 68 minutes. There is more sintering seen in these samples. We can also see nucleation in these samples.

Figure 6.8(C) shows the particles of size 310 μm that were treated at 1000-1020^{0}C. The time of exposure was increased to 120 minutes. Nucleation and crystallization thermal treatment was applied to these samples. The temperature and time exposure used for this thermal treatment was 550^{0}C for 192 minutes, followed by 660^{0}C for 68 minutes. After this treatment as it can be seen in the figure 6.8(C) there is good amount of sintering between the particles. Large particle size leads to high porosity of the materials. Figure 6.8(D) shows the particles of size 310 μm that were treated at 1100^{0}C. The particles were exposed to the thermal treatment for 120 minutes. These samples were then exposed to nucleation and crystallization thermal treatment. The temperature and time exposure used for this thermal

treatment was 550^0C for 192 minutes, followed by 660^0C for 68 minutes. Particles shown in the figure 6.8(D) show very good sintering also, unlike in the particle size 250 µm, porosity of these materials is good. This size will allow good bone regeneration.

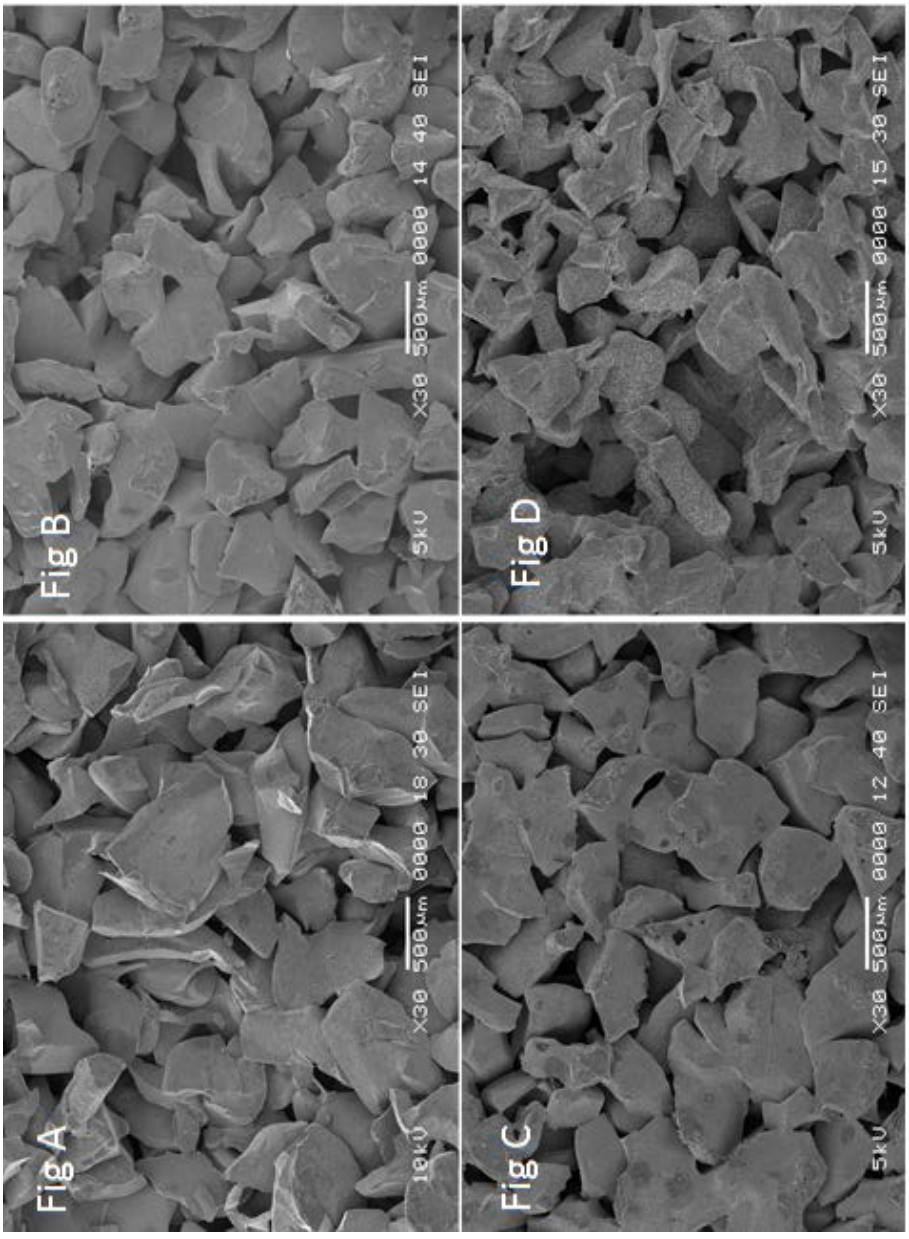

Figure: 6.8 SEM Back scatter Bottom Surface images for 310 µm particle size

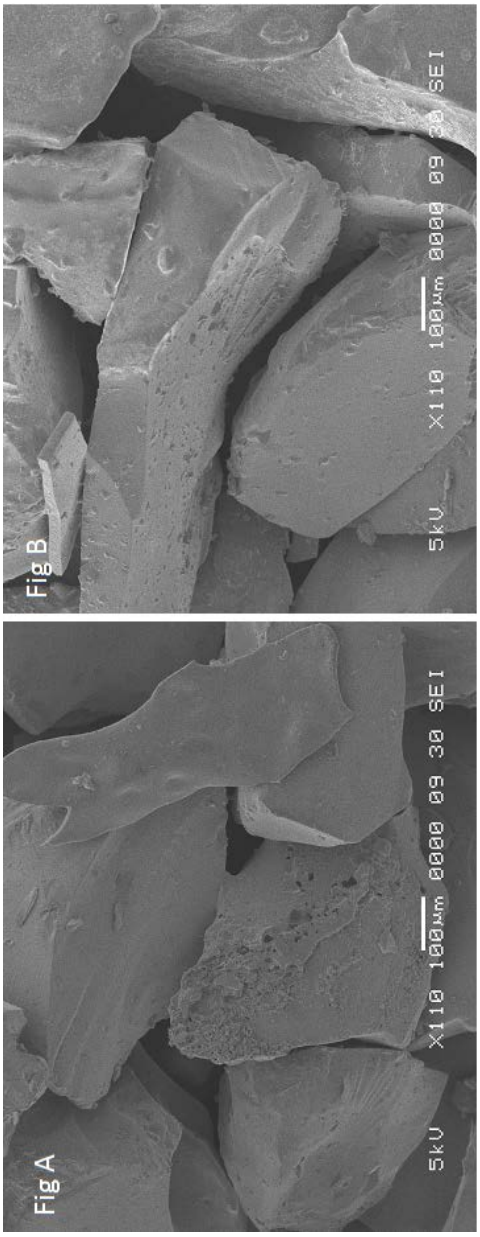

Figure: 6.9 SEM Back scatter images for rapid-slow cooling (Particle size 250 µm)

The size particles Ultrabone glass 310 µm were subjected different sintering temperatures. The figure 6.10 shows backscattered SEM images of the internal layer of the sample.

Figure 6.10(A) shows the particles of size 310 μm that have been treated at 1000-1020^{0}C. There is no sintering is seen in these samples because the time of exposure was only 60 minutes. In the figure 6.10(B) we can see the particles of size 310 μm that were treated at 1000-1020^{0}C. The particles were exposed to the sintering thermal treatment for 120 minutes. These samples were exposed to nucleation and crystallization thermal treatment. The temperature and time exposure used for this thermal treatment was 550^{0}C for 192 minutes, followed by 660^{0}C for 68 minutes. There is no sintering seen in these samples. There is enough porosity in these samples for it to grow, but due to low sintering, strength of the bone is less.

Figure 6.10(C) shows the particles of size 310 μm that were treated at 1000-1020^{0}C. The time of exposure was increased to 120 minutes. Nucleation and crystallization thermal treatment was applied to these samples. The temperature and time exposure used for this thermal treatment was 550^{0}C for 192 minutes, followed by 660^{0}C for 68 minutes. Even after the nucleation and crystallization thermal treatment there is no sintering seen in the internal layers of the surface. Figure 6.10(D) shows the particles of size 310 μm that were treated at 1100^{0}C. The particles were exposed to the thermal treatment for 120 minutes. These samples were then exposed to nucleation and crystallization thermal treatment. The temperature and time exposure used for this thermal treatment was 550^{0}C for 192 minutes, followed by 660^{0}C for 68 minutes. This is the magnified image for figure C. In this figure we can see little amount of sintering. This shows that nucleation

and crystallization thermal treatment has effect on sintering in the internal layer of the samples.

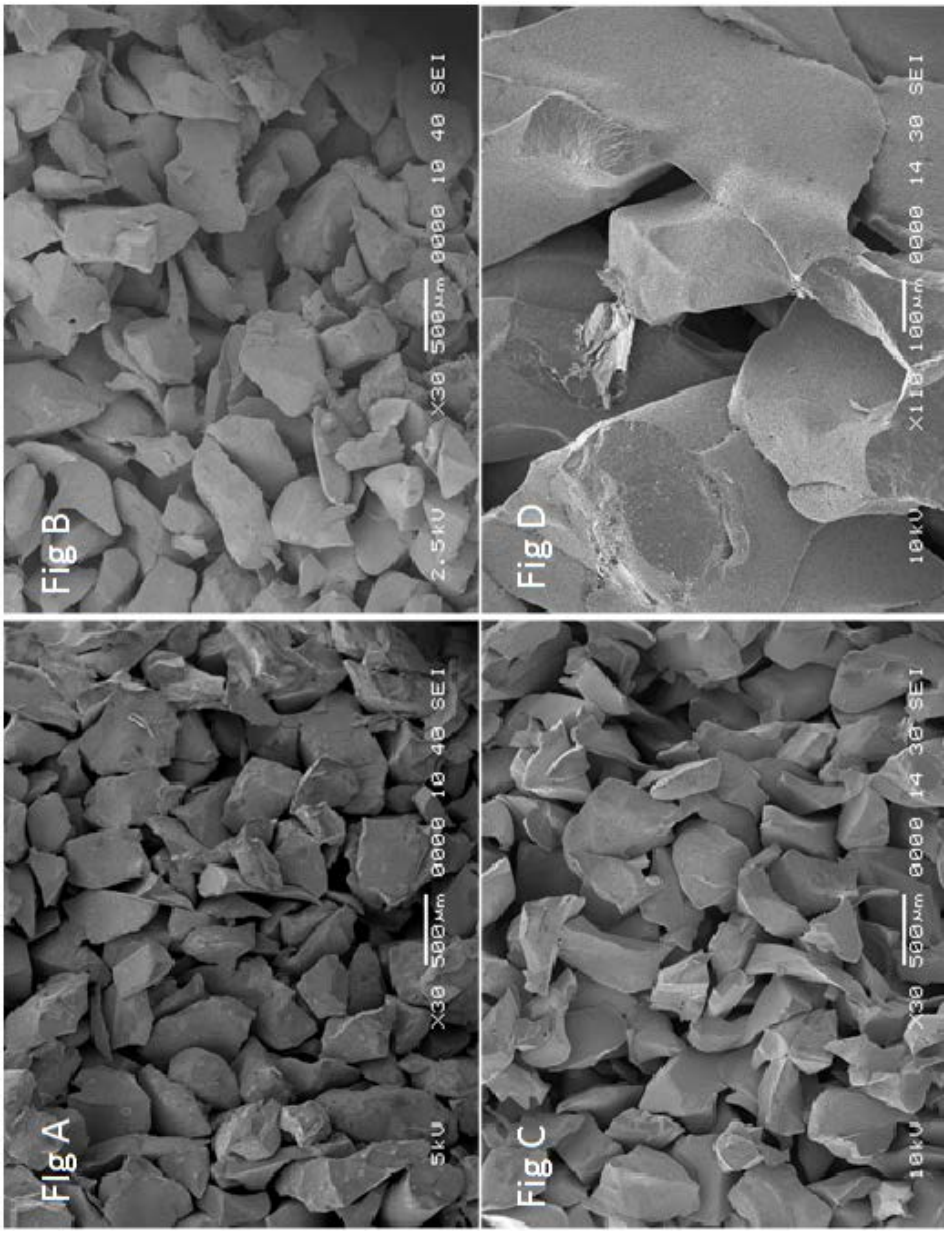

Figure: 6.10 SEM Backscatter Internal Images for 310 µm particle size

The figure 6.11 shows backscattered SEM images of the bottom surface of the sample with particle size 250 μm and 800 μm. All of these samples were also subjected to nucleation and crystallization thermal treatment.

Figure 6.11(A) shows the particles of size 250 μm that have been treated at an increased temperature range 1100-1150^{0}C. The particles have sintered together completely. Porosity is very less in these samples, which means it has very high density. Figure 6.11(B) is a magnified image of figure 6.11(A). We can clearly see higher level of sintering.

In figure 6.11(C) we can see the particles of size 800 μm that were treated at 1100-1150^{0}C. The time of exposure was increased to 120 minutes. Samples were subjected to following nucleation and crystallization thermal treatment, 550^{0}C for 192 minutes, followed by 660^{0}C for 68 minutes. After this treatment as it can be seen in the figure 6.11(C) there is high amount of sintering along with very good porosity. The combination of good sintering and higher porosity facilitates better bone growth. Figure 6.11(D) is the magnified image of the figure 6.11(C). We can clearly see the results discussed in 6.11(C)

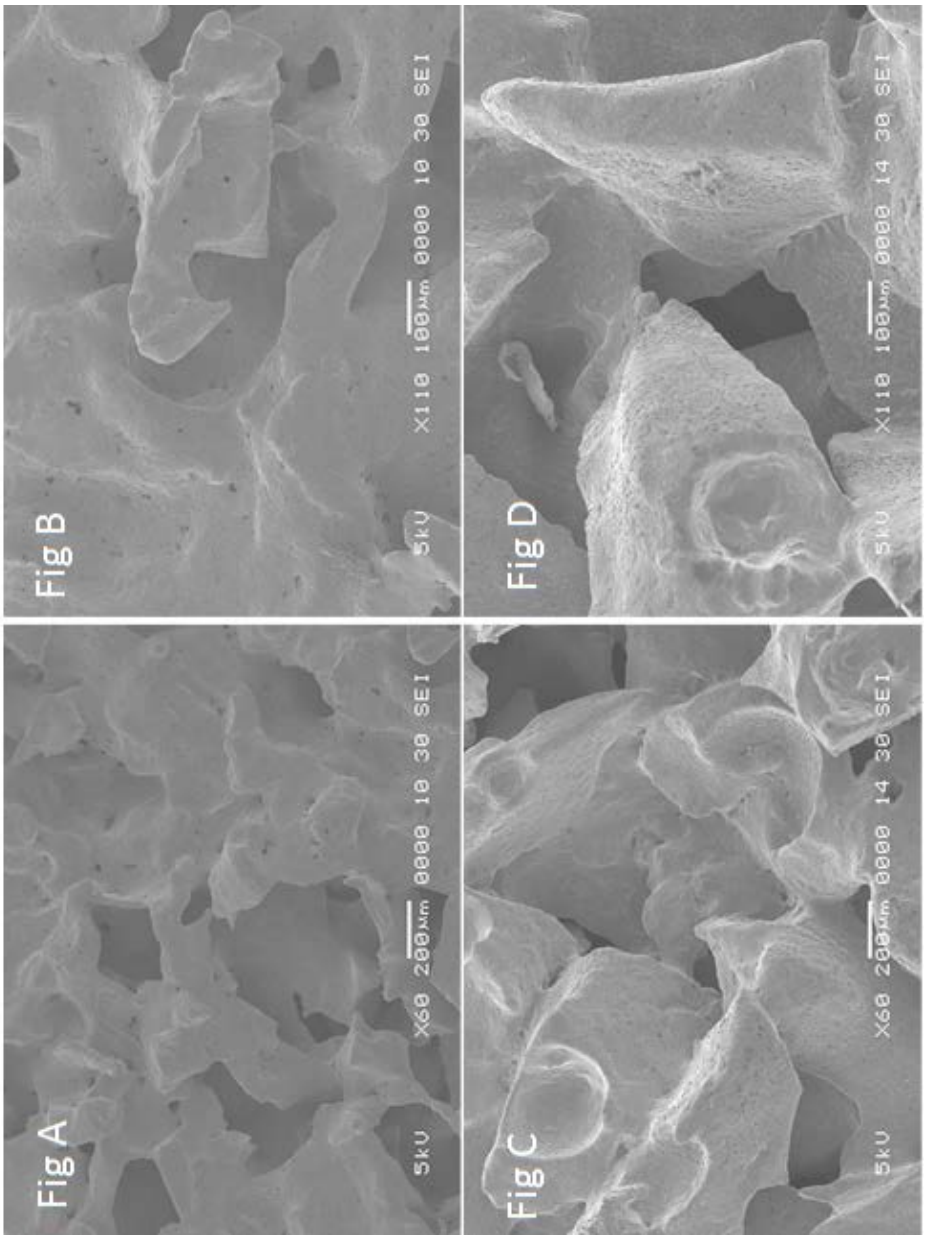

Figure: 6.11 SEM Back scatter images for 250 and 800 µm particle size

6.3 Bioactivity Test (Evaluation of Compatibility)

Any Tissues in biological body which takes up stains are called chromatic. More generalized staining properties, such as acidophilic for tissues that stain by acidic stains (Eosin), basophilic when staining in basic dyes, and amphiphilic that can be stained with either acid or basic dyes. Chromophobic tissues do not take up colored dye readily.

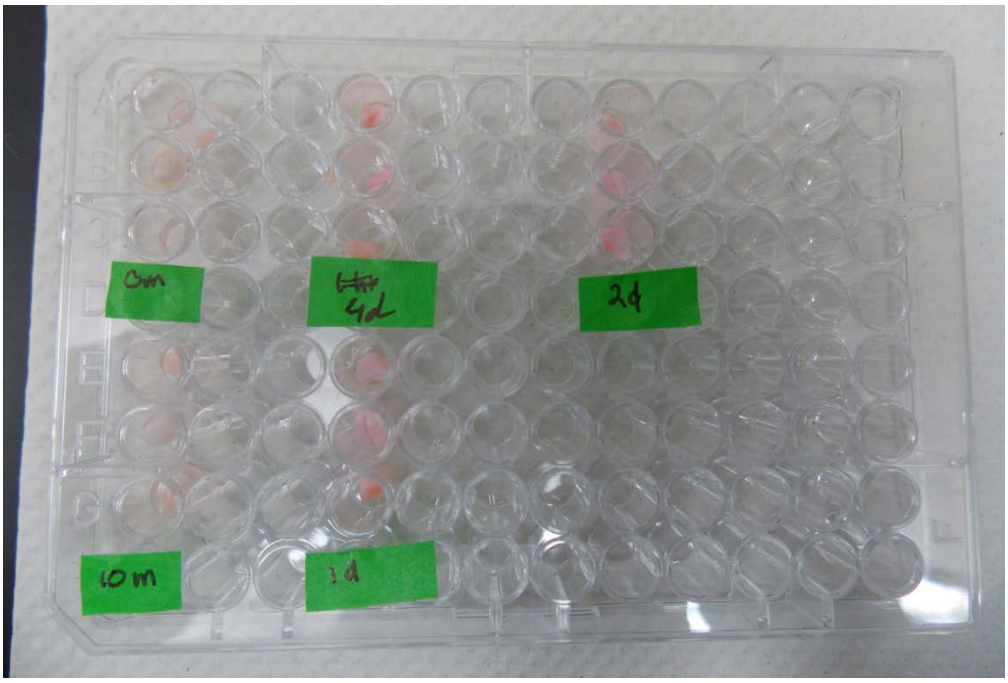

Figure 6.12. Digital Image of Bioactive glass ((3M-Viox 3057)) stain with Eosin

Digital images show results for eosin staining from the bioactive glasses ((3M-Viox 3057)). The control samples do not show any binding with biological stain. It indicates that HCA layer forming does not take place in those samples.

The samples that were taken at 10 minutes time show similar eosin staining as in the control samples. It shows that during first 10 minutes in buffer solution samples HCA layer formation does not take place.

The 1 day and 2 days Samples shows similar and higher intense eosin staining when compared to 10 minutes samples. It indicates formation of HCA layer as time progresses.

The selective blue coloration develops with exposure to air (oxygen) and can be fixed by immersion of the stained specimen in an aqueous solution of ammonium molybdate. Vital methylene blue was formerly much used for examining the innervations of muscle, skin and internal organs.

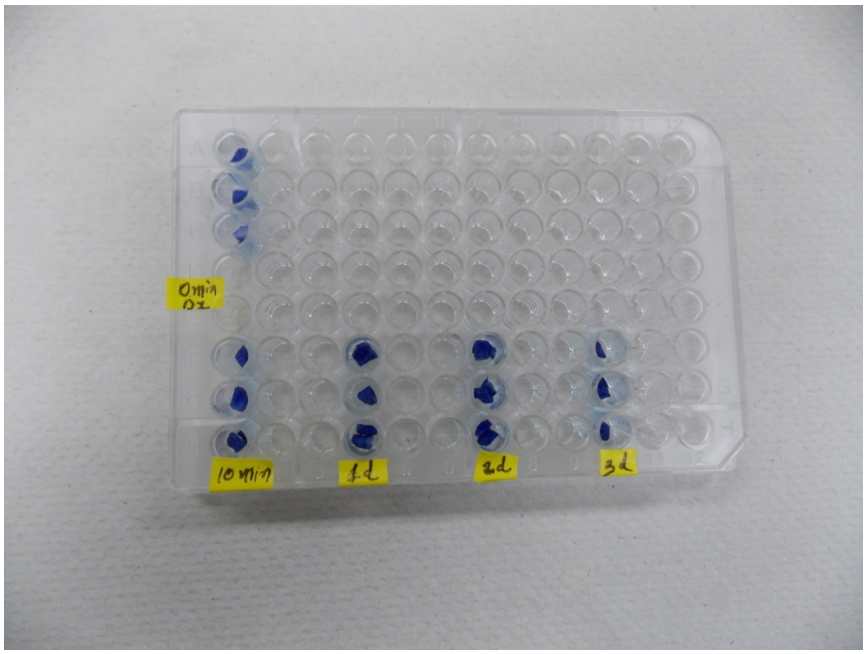

Figure: 6.13 Digital image of bioactive glass ((3M-Viox 3057)) stain with Methylene Blue

Methylene blue is more intense biological stain. In 10 minutes samples should show higher intense stain expression compare to 1 day and following 2 and 3 days. According to this experiment it shows very less difference between samples.

It is very difficult to differentiate stain expression of Methylene blue with naked eyes. From all the staining experiments done it is evident that the sintering affects the biological activity of the bioactive glasses.

6.4 Compression Test (Evaluation of Strength)

In this experiment five samples for each particle size were subjected to compressive strength testing using the INSTRON machine. The 3 KN load cell was used to test the compressive strength of each sample. Each sample was placed between the compression plates as the top plate was lowered until it touched the top of the sample. The rate of compression of 1.0 N/second was placed on each sample until the sample reached its ultimate compression strength value at failure. Graphs of compression strength (MPa) vs. time and Load (N) vs. time were plotted for each sample.

In compression test four different group of bioactive glass with different particle size tested and they shows excellent compressive strength. The group with 800 μm particle sizes prepared in optimal temperature and time has compressive strength approximate 9 MPa. According to the hypothesis, as the

particle size decreases compressive strength increases. This can be seen in the results with particle size 250 μm, maximum compressive strength of 23 MPa was seen. In the samples treated before, compressive strength of 2, 2.7, 4 MPa was also observed. But the highest value of the compressive length was 23 MPa. The samples that we used in this study were cylindrical. The volume of the samples is required to calculate density of the material. The volume was calculated using $\pi r^2 h$. Value of π was taken as 3.14, "r" stands for radius of the circular surface of the cylinder, "h" stands for the height of the cylinder.

Table 2 Density values of bioactive glass samples

Particle size Um	weight of sample g	Height cm	diameter cm	Surface area cm2	Volume cm3	**DENSITY** g/cm3
800	3.2814	1.693	0.55	7.45571	1.60809	**2.0405**
650	2.945	1.56	0.55	6.87006	1.4817	**1.98749**
310	2.66	1.43	0.54	6.15875	1.30943	**2.0315**
250	2.866	1.339	0.53	5.63776	1.18103	**2.4266**

Initially we used particle size of 250 μm temperatures from 650-800^{0}C. In this temperature range, we did not get any sintering in any samples. The samples treated at this temperature were very brittle and would disintegrate very easily. This is supported by the SEM image for this test [Figure 6.6(A)]. Later we increased the temperature to 1000-1020^{0}C. When the samples were treated at this temperature, sintering was better than the previous temperature, but the sample was

in the form of rectangular block and it got stuck to the walls of the ceramic boats. This is also seen in the SEM image of [Figure 6.6(C)]. Dremel tools were used to cut the samples out from the ceramic boats. The samples taken were loaded on Instron and mechanical properties were recorded. As seen in the figure 6.14, the compressive strength for this treatment was found to be 5.32 MPa, which shows a strong material stress-strain curve.

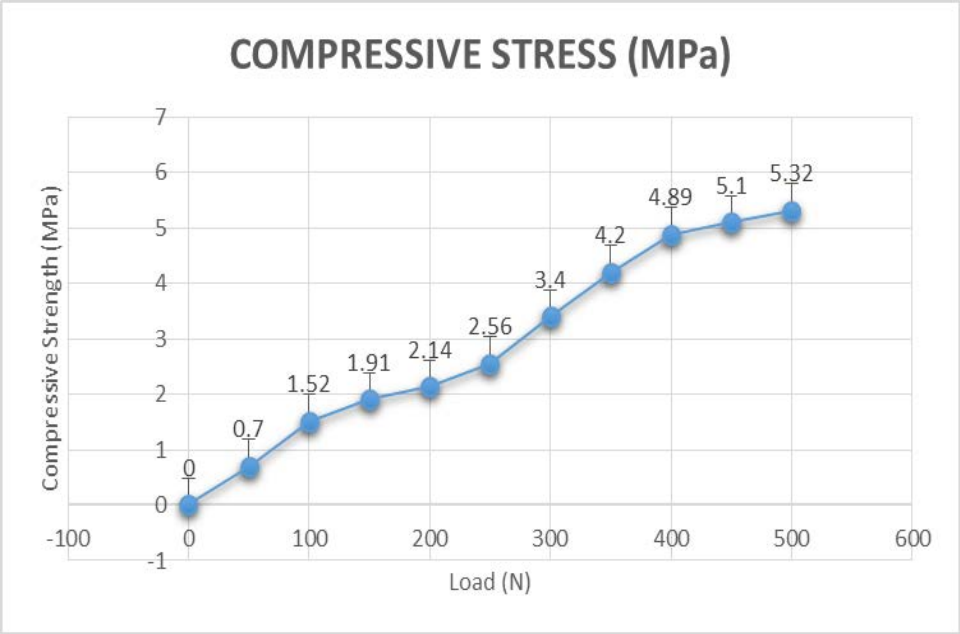

Figure 6.14 shows Compressive strength curve for 250 µm particle

Next particle size chosen for tests was 310 µm. These samples were first sintered at 1000-1020^{0}C. In this we got good sintering, the compressive strenth was found to be 4.43 MPa (Figure 6.15A). The same sample was subjected to 1100^{0}C for sintering. The samples were not subjected to nucleation. The samples still showed increased Compressive strength, 13.65 MPa (Figure 6.15B)

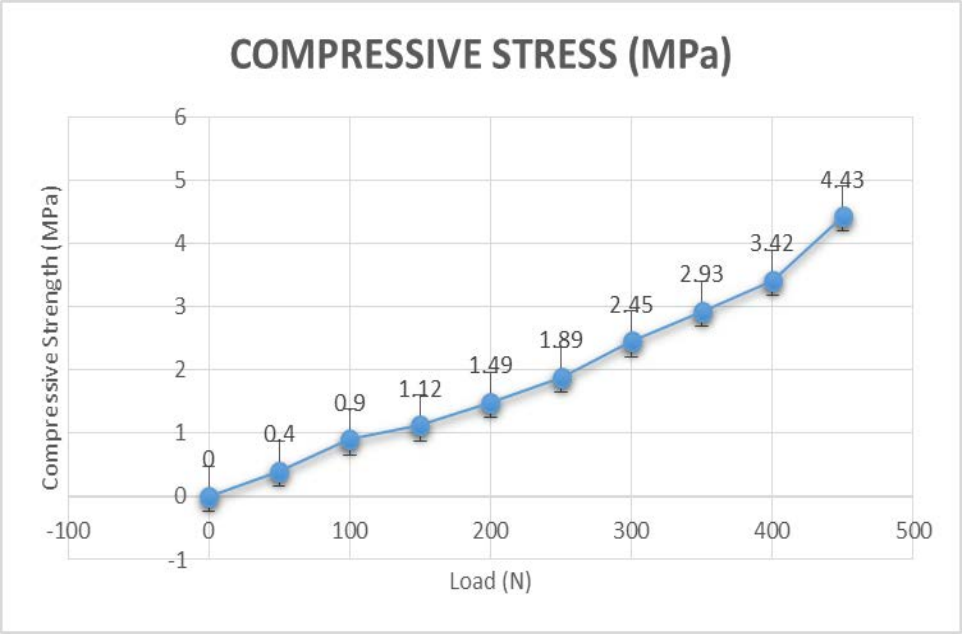

Figure 6.15(A) compressive strength versus load graph of the particle size 310 µm

The sample particle size for the following figures was 650 µm. The sintering was done at 1000-1020^{0}C. This temperature was found to be optimum and showed good sintering. There were two parts of the sample. One part was not subjected to the nucleation thermal treatment, the other one was subjected to the nucleation thermal treatment. The samples after the thermal treatments were analyzed for its mechanical strength using Instron. Graphs in figure 6.16A) and 6.16(B) were plotted using compressive strength and load values. As seen from the graph the material that was subjected to the nucleation thermal treatment showed higher compressive strength (4.87 MPa) than the one that was not nucleated (2.287 MPa).

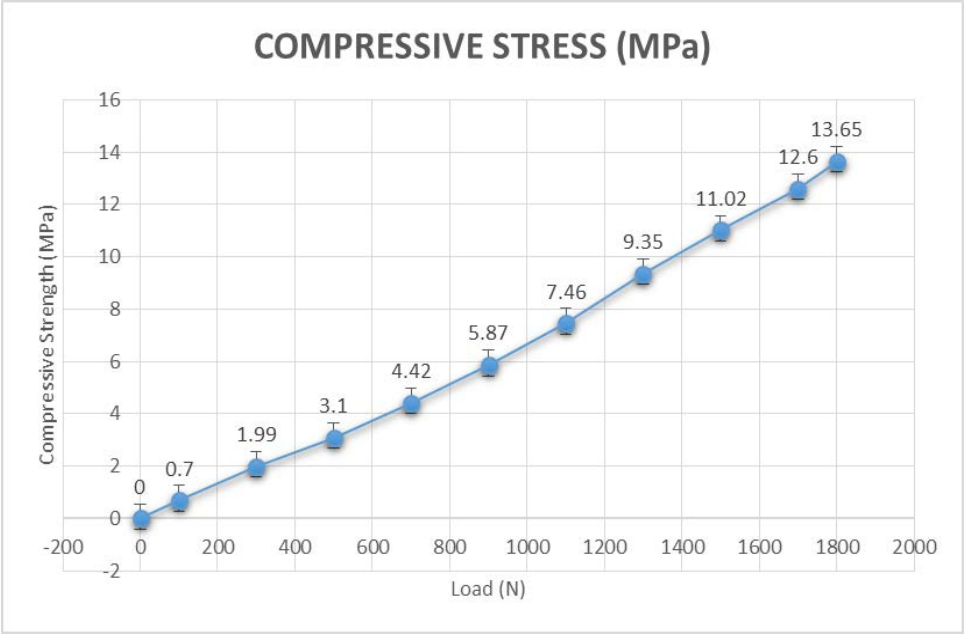

Figure 6.15(B) compressive strength versus load graph of the particle size 310 µm sintered at 1100^0C

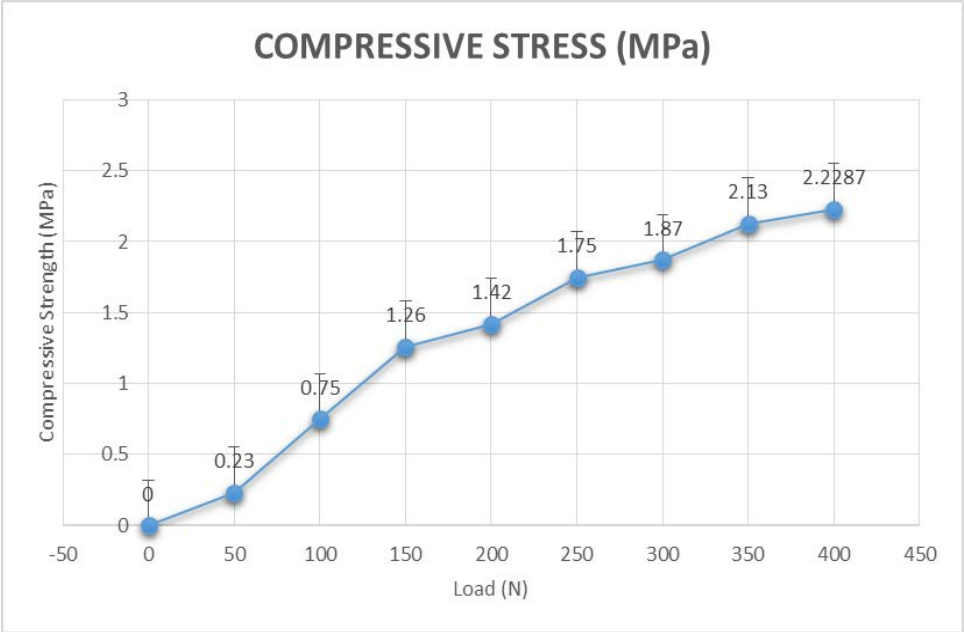

Figure 6.16(A) Compressive strength versus load graph of the sample not subjected to nucleation.

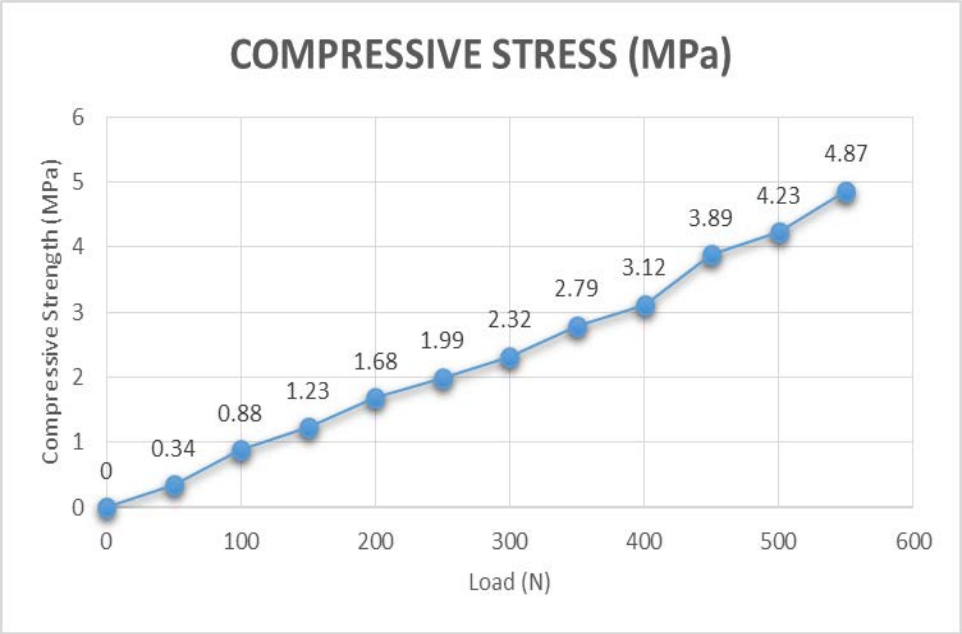

Figure 6.16 (B) Compression versus load curve for particle size 650 µm. subjected to nucleation thermal treatment.

The next test includes sintering of the particle size 250 µm at 1100^0C. These particles were then analyzed using Instron. The compressive strength for these samples was found to be the highest (22.47 MPa) as shown in figure 6.17. Even after having the maximum compressive strength, these particles are not a good candidate for bone regeneration because there is a loss of porosity to a greater extent. Good sintering and no porosity can also be seen in the SEM image of this treatment [Figure 6.6 (D)]. There is a drop in the compressive strength of the sample; it is because when Instron was applying load there was a crack in the sample. The crack did not break the material completely, just introduced a sudden drop in the value of compressive strength.

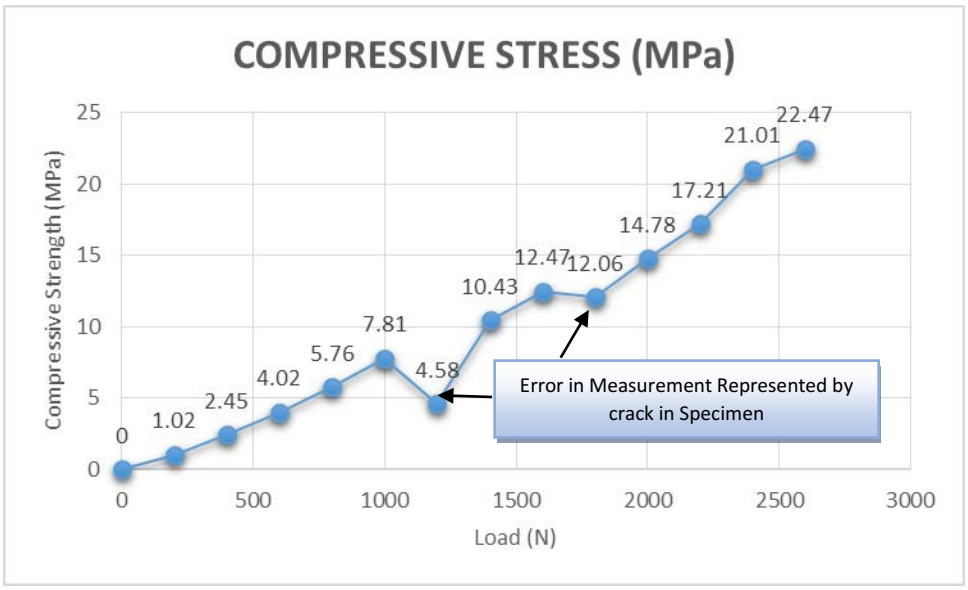

Figure 6.17 Compressive strength versus load graph for particle size 250 µm at 1100^0C

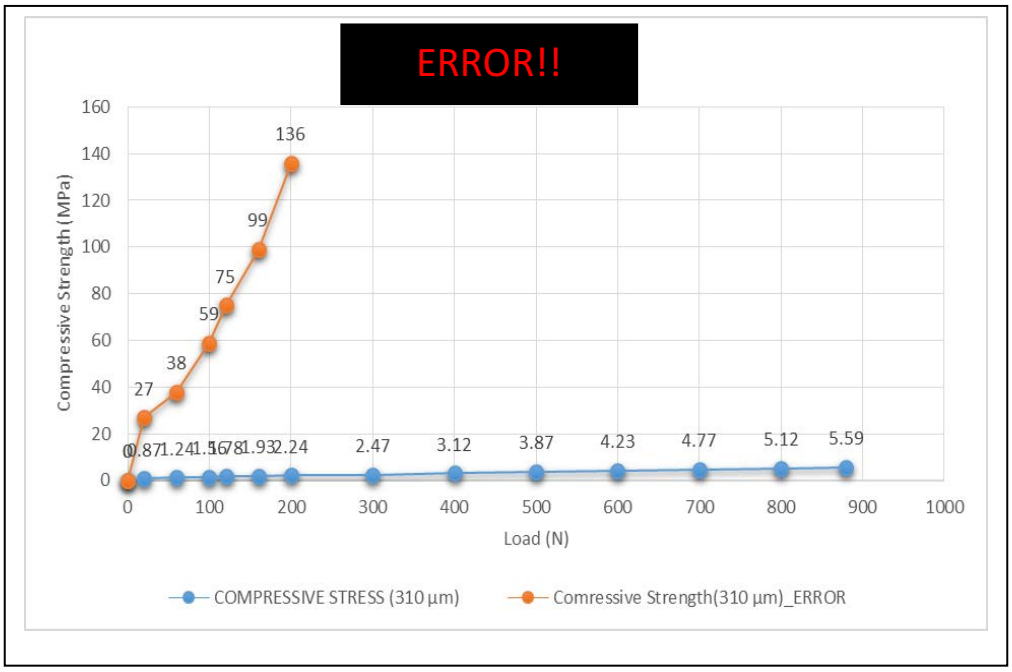

Figure 6.18 Error in measurement

The figure 6.18 represents the error in our measuring protocol. When the readings were taken for the first time there was no connection between the load plate and transducer. As we can see for the red line, compressive strength reaches 136 MPa in only 100 N. After this error was corrected we got normal compressive strength value of 5.59 MPa. It shows good amount of compressive strength in this graph as the load on the specimen is increased. The internal force of the material opposes the external load applied load, so the curve should increase exponentially. There is a sudden decrement seen in the figure at 1000 N. The compressive strength starts increasing again; this shows error in the measurement. This error is physically represented by a big crack in the specimen.

After experimenting with the different sintering temperatures we came to conclusion that 1100^0C was the optimum temperature for good sintering, porosity, and mechanical strength. The sintering treatment at 1100^0C gives maximum sintering, increase in density. Increment in the density leads to increased compressive strength that is closer to the cortical bone. After finding out the optimum temperature we changed the size of the particle keeping the temperature constant at 1100^0C. The samples treated under these conditions, were analyzed using Instron and the graph of compressive strength versus load were plotted [Figure 6.19-6.22].

The particle size used to plot this graph is 800 µm. The particle size was higher size so the materials sintered well when exposed to high temperature.

Strength increased with the sintering treatment. Maximum strength was found to be 9.2 MPa as shown in figure 6.19. The density of these samples was 2.0405 g/mm^3.

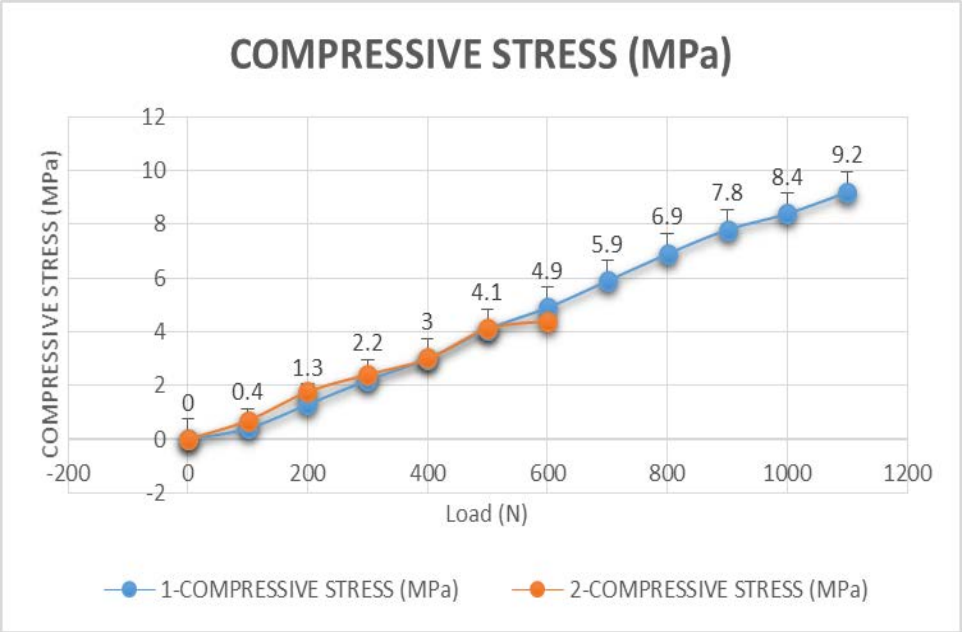

Figure 6.19 Compressive strength versus load graph for particle size 800 µm at 1100^{0}C

As in Fig 6.20 shows the particle size used to plot this graph is 650 µm. The particle size was higher size so the materials sintered well when exposed to high temperature. Strength increased with the sintering treatment. Maximum strength was found to be 11.9 MPa. The density of these samples was 1.98749 g/mm^3. These samples had the lowest strength.

As in Fig 6.21 shows the particle size used to plot this graph is 310 µm. The particle size was higher size so the materials sintered well when exposed to high temperature. Strength increased with the sintering treatment. Maximum

strength was found to be 12.89 MPa. The density of these samples was 2.0315 g/mm^3.

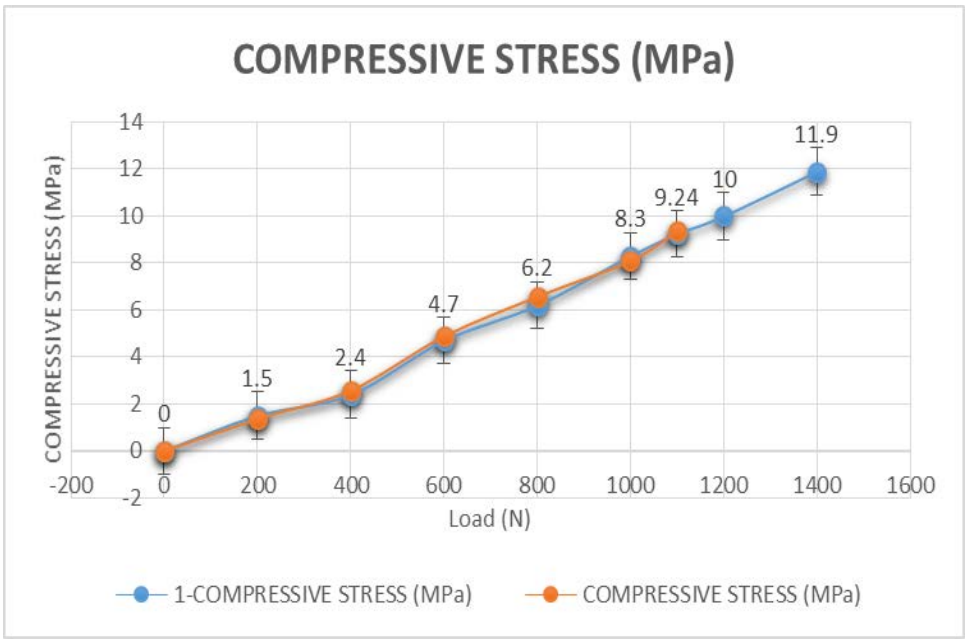

Figure 6.20 Compressive strength versus load graph for particle size 650 µm at 1100^{0}C

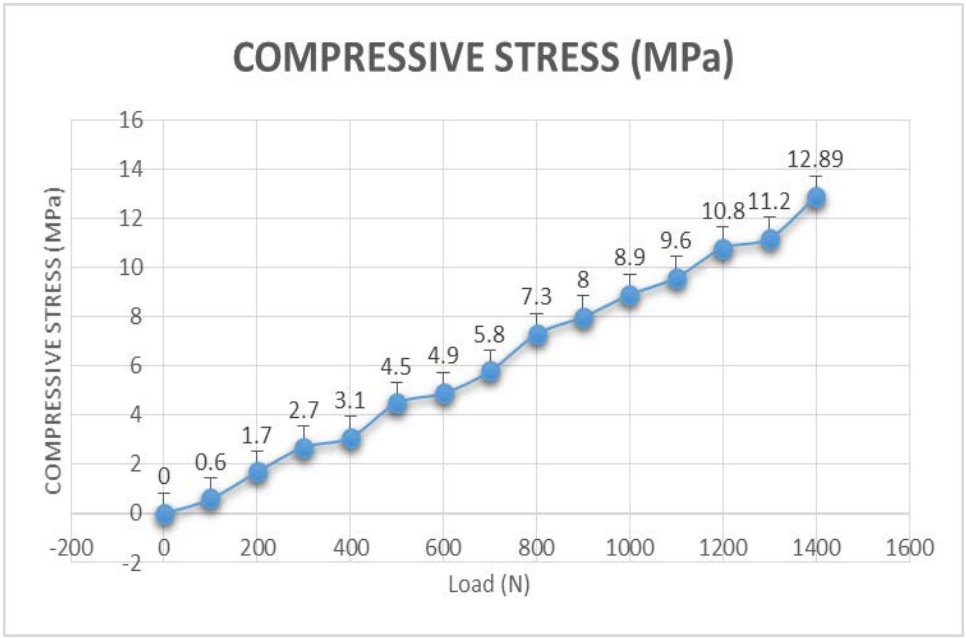

Figure 6.21 Compressive strength versus load graph for particle size 310 µm at 1100^{0}C

As in Fig 6.22 shows the particle size used to plot this graph is 250 µm. The particle size was lower size so the materials sintered well when exposed to high temperature. Strength increased with the sintering treatment. Maximum strength was found to be 24 MPa. The density of these samples was 2.4266 g/mm^3.

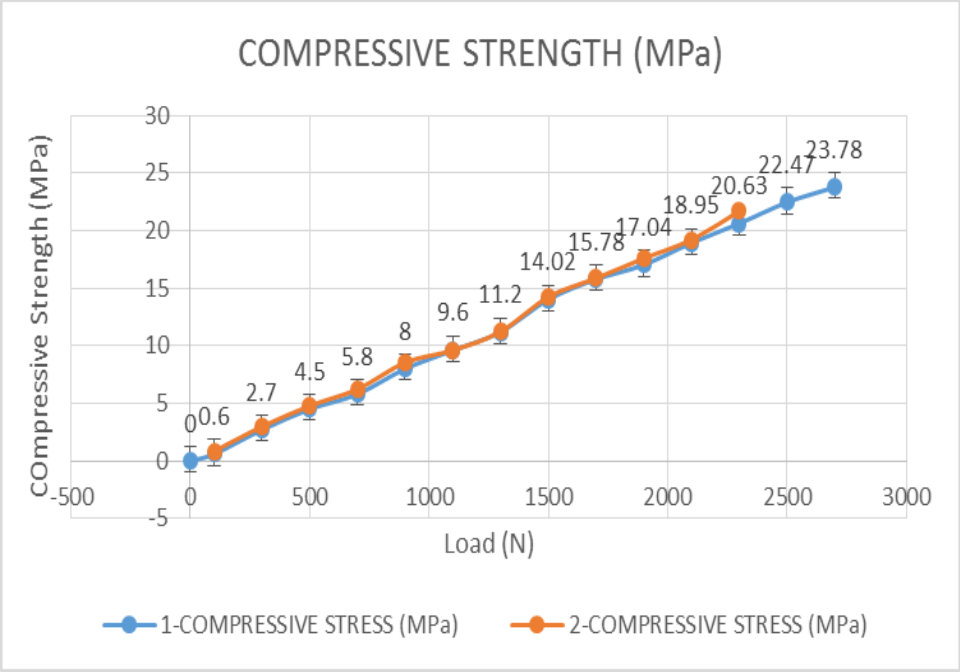

Figure 6.22 Compressive strength versus load graph for particle size 250 µm at 1100^{0}C

The graphs plotted with the help of the data collected from the experiments done on the samples sintered using different sintering treatments show that there is a significant difference in the density and compressive strength. This further helps us prove the hypothesis.

CONCLUSION

In this study, Ultrabone glass composition 3MViox-3057 (Hench et. al patent) glass frit was exposed different sintering treatment. The exposure temperature and time were differed, and it was observed that there is change in porosity, density, mechanical properties. The crystallization and nucleation improve the mechanical properties, but affect the surface bioactivity of the samples.

There are two aims stated at the beginning. First aim is to get mechanical properties identical to the cortical bone; second aim was to get biocompatibility similar to bioactive glasses 45S5. Shape and size distribution of the particle and the inclusion distribution in the matrix play an important role in enhancing the mechanical properties of the bioactive glasses. Platelet or particle or even powder form of the bioactive glasses are often used as bone defect filler or dental implants, cranial, and maxillofacial reconstruction. Ongoing transformation in the glass structure influences the sintering behavior of the 3MViox-3057. In this process three stages were identifies. First stage of rapid densification takes place from 550-670^{0}C. The samples pile up together, show very less sintering and did not come out as a whole block. This takes place when glass-in-glass phase separation and crystallization takes place. When the temperature is increased to 670-900^{0}C, better sintering is observed. To begin with the samples were treated at a low temperature range 550-800 C. In these samples, very less amount of sintering was observed. The temperature was then increased up to 900 C, at this temperature partial sintering was observed with rapid and slow cooling techniques. The third

and important stage of the densification takes place above 950^0C. After increasing the temperature to 1000-1020^0C, sintering was found to be better than the previous temperatures. At this temperature, the sintered particles stuck to the walls of the ceramic boats. The particles did not come out as one block and hence, could not be used for further mechanical testing. To overcome this problem, walls of the ceramic boats were coated graphite spray. Graphite spray did not help with the particles getting stuck so, instead of ceramic boats, graphite bricks were used. Using graphite bricks helped removing the samples but sintering was not that good. The densification occurs faster at the temperatures above 1000^0C. The density of sample increases very rapidly; which leads to increase in the compressive strength. In the paper published by Dr. Dutta and Bose, they show how the density of the sample increases with the temperature [84]. We got similar results with our materials. In the figure 9, of the paper published by Hashmi, M.U et. al., we can see the density versus graph that also shows the similar results as what we got [85]. Rapid increase in the compressive strength can be seen in figure 6.13 and 6.14(A). These figures show the effect of sintering temperatures on the strength of the bioactive glasses. Good sintering was achieved at 1100 C. At this temperature, the sample particle size was too low (250 μm). Low particle size resulted in low porosity; Figure 6.21 shows the effect of the sintering temperature on the compressive strength of the bioactive glasses (23 MPa), but figure 6.11(B) shows how the samples loose porosity. After the particle size was increased and treated at 1100 C good porosity, density, and good compressive strength was obtained. Figure 6.18 shows the how

sintering leads to compressive strength (9.2 MPa) with the large particle size 800 μm. Figure 6.11(D) shows how the samples also remain porous.

There are three categories of the biological stains. Acidic stains that stain the acidophilic tissues, basic stains that stain the basophilic tissue and amphophilic the tissues that can be stained by both acidic and basic stains. The second aim of the study was tested using biological stains namely, eosin and methylene blue. In this process eosin is the acidic stain and methylene blue is the amphiphilic stain. These biological stains bind to the Hydroxy Carbonate Apatite layer. The bioactivity of the bioglasses could be substantially suppressed by crystallization. The amount of the amorphous phase retained by the bioactive glass affects the ability of the bioactivity to form HCA layer. The glassy phase that is abundantly immersed in the simulated physiological solution will promote the formation of HCA layer on top of the silicon rich layer. In almost completely crystallized material, only a silica rich material was observed. This suggests that there is precipitation of the apatite depending on the presence of residual glassy phase in the bioactive glass. Samples used for bioactivity tests were treated at 1000-1020^{0}C. Eosin binds to the cations leaching from the HCA layer and methylene blue binds to the negatively charged HCA layer. From the staining tests performed on these samples we got that eosin and methylene blue stain the samples significantly. The staining of these samples is shown in the figures 6.12 and 6.13. The samples were stained with eosin using the protocol explained in the methods, the samples that were stained for 10 minutes showed almost same intensity of

staining as in the control. The samples taken out after 1 day and 2 days showed increased intensity of staining. Lack of staining in the 10 minutes sample and increased staining after 1 day and 2 day respectively indicates HCA layer formation took place. The samples were also stained with methylene blue. Methylene blue is more intense biological stain. The samples taken out after 10 minutes should show more staining than the ones that were taken out after 1 day, 2 day, and 3 day period. The stain expression of methylene between different samples did not show much difference. But the expression of methylene blue is difficult to examine, as they showed very less difference. Other techniques used to quantify the bioactivity are Fourier Transform Infrared Spectroscopy (FTIR), cell based proliferation technique [86, 87, and 88]. Hench hypothesis states that even if the composition of the bioactive glasses is changed, there is some formation of the HCA layer [83]. Dr. Larry Hench proposed a hypothesis," Even though the composition of bioactive glasses synthesized is quite different, it seems that the mechanism of HCA formation involves some specific steps that are analogous for all of them". 3M-ViOx-3057 follows the Hench hypothesis [83, 84]. There is activity seen when the eosin is used, but it is very difficult to detect the bioactivity without FTIR, cell based proliferation technique. The particles were temperature above 1100^0C for more than 120 minutes sintered well. The compressive strength increased to greater extent. The dramatic increase in the compressive strength of the particles came along decreased biocompatibility owing to the inner matrix phase. This can be seen in the figure 6.11.

Bioactive materials have been used to suffice the need of tissue replacement for a long time now. Evolving techniques have made these materials more versatile and their utility has increased a lot. The third generation bioactive glasses are now a day porous and activate genes that stimulate tissue growth. The heat treatment that was used in the experiments I performed was observed to enhance the porosity, and compatibility of the bioactive glasses till a level that they enhance the regeneration of the living tissue. The mechanical properties of the bioactive materials when subjected to the sintering treatments were increased to be similar to the cortical bones; which allows the bioactive materials to fill the defects in the bones. The next improvement that will lead to a great improvement of the bioactive glasses in incorporation of the nano particle scaffolds that mimic the extra cellular matrix of the tissue.

According to the hypothesis, "different thermal treatments will show improvement in mechanical properties and biological response of these of Ultrabone glasses 3MVioX-V3057. The sintering treatment will improve the mechanical properties similar to the natural cortical bone", thermal temperatures selected have an effect on sintering. Changes in the sintering change the densification of the material. The densification improves the compressive strength of the materials. The maximum compressive strength was seen at the optimal temperature and optimal exposure time. As we do not have the X-Ray diffraction facility at our institute, we had to take help of crude methods of detecting bioactivity. Further investigations using Raman spectroscopy on the results

obtained from eosin and methylene blue bioactivity test need to be done in order to have correct quantification of the bioactivity [89].

FUTURE DIRECTION

The amount of the sintering increased every time temperature and time of exposure was increased. But porosity needs to be controlled too. For future studies, we would like to find an optimum temperature for sintering and still be able to maintain the porosity for the particle sizes 600 μm and 800 μm. The compressive strength of the material that we have to achieve is 50 MPa. This is the compressive strength equivalent to the transverse cortical bone strength. We would also like to study the samples we made using X-Ray crystallography techniques. The X-Ray crystallography is based on the diffraction of the X-Rays. It is used to measure the size of the particle, depending on the amount of diffraction, and angle of diffraction. This will give us a better view of the bioactivity of the material. The glass that was immersed abundantly in the simulated physiological solution helped the formation of HCA layer on the surface of the silicon rich layer. In case of the completely crystallized materials, only silica rich layer was observed. This suggests that, in bioactive glasses, the precipitation of the apatite depended on the presence of residual glassy phase. Increasing the sintering temperature above 1200^0C 3MViox-3057 lost its crystalline structure and melted completely. Using larger particles and treating them in the temperature range of 1000-1150^0C would help us overcome this problem. Using this strategy, we hope to get better sintering, porosity, and biocompatibility.

Tension test is the most common type of the test used to measure the mechanical properties of the materials. It gives us information on the strength of

the materials. It is also an acceptance test for specification of the materials. Tensile strength, yield strength or yield point, elastic modulus, percent elongation and reduction in area are some of the major parameters that describe the stress-strain curve. This testing technique also gives information on toughness, resilience, Poisson's ratio. The next part of the future goals include, checking the tensile strength.

The next goal to be achieved in future is to check tensile strength of the bioactive materials. Tensile strength can be checked using the same instrument Instron and the bluehill software. The shape and tensile strength of the material is important because we have to avoid the samples from breaking and fracture within the area that is being gripped. The cross sectional area of the material should be as low as it can be.

The most important property of the materials is the modulus of elasticity. It describes its stiffness. The modulus of elasticity can be calculated using stress/strain. The values of stress and strain can be obtained from the tensile curves and can be applied to calculate the modulus of elasticity.

REFERENCES

1. An Introduction to Bioceramics (2nd Edition), L.L.Hench Copyrights © 2013 by Imperial College Press.
2. Hench, L. L., and Polak, J. M. (2002). Third-generation biomedical materials. Science, 295(5557), 1014-1017.
3. Oreffo, R. O. C., and Triffitt, J. T. (1999). Future potentials for using osteogenic stem cells and biomaterials in orthopedics. Bone, 25(2), 5S-9S.
4. *Zambonin*, G., and Grano, M. (1995). Biomaterials in orthopaedic surgery: effects of different hydroxyapatites and demineralized bone matrix on proliferation rate and bone matrix synthesis by human osteoblasts. *Biomaterials*, *16*(5), 397-402.
5. Furth, M. E., Atala, A., and Van Dyke, M. E. (2007). Smart biomaterials design for tissue engineering and regenerative medicine. Biomaterials, 28(34), 5068-5073.
6. Rezwan, K., Chen, Q. Z., Blaker, J. J., and Boccaccini, A. R. (2006). Biodegradable and bioactive porous polymer/inorganic composite scaffolds for bone tissue engineering. Biomaterials, 27(18), 3413-3431.
7. Wang, Min. "Developing bioactive composite materials for tissue replacement." Biomaterials 24, no. 13 (2003): 2133-2151.
8. Omori, K., Nakamura, T., Kanemaru, S., Asato, R., Yamashita, M., Tanaka, S. and Shimizu, Y. (2005). Regenerative medicine of the trachea: the first human case. Ann Otol Rhinol Laryngol, 114(6), 429-433.
9. Duke University. (2014, February 18). Regenerating orthopedic tissues within the human body. ScienceDaily. Retrieved November 5, 2014 from www.sciencedaily.com/releases/2014/02/140218185104.htm
10. Hench, L. L., Xynos, I. D., and Polak, J. M. (2004). Bioactive glasses for in situ tissue regeneration. Journal of Biomaterials Science, Polymer Edition, 15(4), 543-562.
11. Mahoney, M. J., and Saltzman, W. M. (2001). Transplantation of brain cells assembled around a programmable synthetic microenvironment. Nature biotechnology, 19(10), 934-939.
12. Brach del Prever EM, Donati DM, Fiorentino S, Macrì E. Regulatory aspects of regenerative medicine products and informed consent GIOT 2010; 36 p. 223-242.
13. Vögelin E, Jones NF, Huang JI, Brekke JH, Lieberman JR. Healing of a criticalsized defect in the rat femur with use of a vascularized pe- riosteal flap, a biodegradable matrix, and bone morphogenetic pro- tein. J Bone Joint Surg Am. 2005;87:1323-31.

14. Burkoth AK, Burdick J, Anseth KS. Surface and bulk modifications to Photocrosslinked polyanhydrides to control degradation behavior. J Biomed Mater Res. 2000;51:352-9.
15. Lee KW, Wang S, Lu L, Jabbari E, Currier BL, Yaszemski MJ. Fabricationand characterization of poly(propylene fumarate) scaffolds with controlled porestructures using 3-dimensional printing and injec- tion molding. Tissue Eng. 2006;12:2801-11
16. Alvarez, K., and Nakajima, H. (2009). Metallic scaffolds for bone regeneration. Materials, 2(3), 790-832.
17. Jacobs, J.J.; Skipor, A.K.; Patterson, L.M.; Hallab, N.J.; Paprosky, W.G.; Black,J.; Galante, J.O. Metal release in patients who have had a primary total hip arthroplasty. J. Bone Joint Surg. Am.1998, 80, 1447-1458.
18. Hench, L. L. (2006). The story of Bioglass®. Journal of Materials Science: Materials in Medicine, 17(11), 967-978.
19. Farooq et al., 2012 I. Farooq, Z. Imran, U. Farooq, A. Leghari, H. Ali. Bioactive glass: a material for the future World J. Dent., 3 (2) (2012), pp. 199–201.
20. G. Hastings and P. Ducheyne (Eds), Macromolcular Biomaterials. CRC Press, Boca Raton, FL (1984).
21. Hench, L. L., Splinter, R. J., Allen, W. C., and Greenlee, T. K. (1971). Bonding mechanisms at the interface of ceramic prosthetic materials. Journal of Biomedical Materials Research, 5(6), 117-141.
22. Beckham, C. A., Greenlee Jr, T. K., and Crebo, A. R. (1971). Bone formation at a ceramic implant interface. Calcified Tissue Research, 8(1), 165-171.
23. Cao, W., and Hench, L. L. (1996). Bioactive materials. Ceramics international, 22(6), 493-507.
24. Hench, L. L., and Polak, J. M. (2002). Third-generation biomedical materials. Science, 295(5557), 1014-1017.
25. L. L. Hench, Science 208, 826 (1980)
26. Wilson, J., and Low, S. B. (1992). Bioactive ceramics for periodontal treatment: comparative studies in the Patus monkey. Journal of Applied Biomaterials, 3(2), 123-129.
27. Compositional and microstructural design of highly bioactive P2O5–Na2O–CaO–SiO2 glass-ceramics by Oscar Peitl a, Edgar D. Zanotto a, Francisco C. Serbena b, Larry L. Henchc ; Acta Biomaterialia 8 (2012) 321–332
28. Bone Structure and Function. (n.d.). Retrieved November 6, 2014.
29. Brandi, M. L. (2009). Microarchitecture, the key to bone quality. *Rheumatology*,*48*(suppl 4), iv3-iv8.

30. Dempster, D. W., Lian, J. B., and Goldring, S. R. (2006). Anatomy and functions of the adult skeleton. *Primer on the metabolic bone diseases and disorders of mineral metabolism*, *6*, 7-11.
31. Bao, C. L. M., Teo, E. Y., Chong, M. S., Liu, Y., Choolani, M., and Chan, J. K. (2013). Advances in bone tissue engineering. Regenerative medicine and tissue engineering. Rijeka: Intech, 599-614.
32. Clarke, B. (2008). Normal bone anatomy and physiology. Clinical journal of the American Society of Nephrology, 3(Supplement 3), S131-S139.
33. Carlson, B. M. (2004). Human embryology and developmental biology. Mosby Inc.
34. Smith, M. M., & Hall, B. K. (1993). A developmental model for evolution of the vertebrate exoskeleton and teeth. In Evolutionary biology (pp. 387-448). Springer US.
35. Kronenberg, H. M. (2003). Developmental regulation of the growth plate. *Nature*,*423*(6937), 332-336.
36. Hunziker, E. B., Schenk, R. K., and Cruz-Orive, L. M. (1987). Quantitation of chondrocyte performance in growth-plate cartilage during longitudinal bone growth. The Journal of Bone and Joint Surgery, 69(2), 162-173.
37. Ubara, Y., Tagami, T., Nakanishi, S., Sawa, N., Hoshino, J., Suwabe, T., ... and Takaichi, K. (2005). Significance of minimodeling in dialysis patients with adynamic bone disease. Kidney international, 68(2), 833-839.
38. Ubara Y, Fushimi T, Tagami T, Sawa N, Hoshino J, Yokota M, Kaitori H, Takemoto F, Hara S: Histomorphometric features of bone in patients with primary and secondary hyperparathyroidism. Kidney Int 63: 1809 –1816, 2003
39. Lindsay R, Cosman F, Zhou H, Bostrom M, Shen V, Cruz J, Nieves JW, Dempster DW: A novel tetracycline labeling schedule for longitudinal evaluation of the short-term effects of anabolic therapy with a single iliac crest biopsy: Early actions of teriparatide. J Bone Miner Res 21: 366 –373, 20
40. Kobayashi S, Takahashi HE, Ito A, Saito N, Nawata M, Horiuchi H, Ohta H, Ito A, Iorio R, Yamamoto N, Takaoka K: Trabecular minimodeling in human iliac bone. Bone 32:163–169, 2003
41. Teitelbaum, S. L. (2000). Bone resorption by osteoclasts. Science, 289(5484), 1504-1508.
42. The Editors of Encyclopædia Britannica. (n.d.). Osteoblast (cell). Retrieved November 6, 2014.
43. Purves et al., Life: The Science of Biology, 4th Edition]
44. Solheim, E. (1998). Growth factors in bone. International orthopaedics, 22(6), 410-416.

45. Linkhart, T. A., Mohan, S., and Baylink, D. J. (1996). Growth factors for bone growth and repair: IGF, TGFβ and BMP. Bone, 19(1), S1-S12.
46. Dimitriou, R., Jones, E., McGonagle, D., and Giannoudis, P. V. (2011). Bone regeneration: current concepts and future directions. BMC medicine, 9(1), 66.
47. Giannoudis, P. V., Dinopoulos, H., and Tsiridis, E. (2005). Bone substitutes: an update. Injury, 36(3), S20-S27.
48. Finkemeier, C. G. (2002). Bone-grafting and bone-graft substitutes. The Journal of Bone and Joint Surgery, 84(3), 454-464.
49. Carter, D. R., Schwab, G. H., and Spengler, D. M. (1980). Tensile fracture of cancellous bone. *Acta Orthopaedica*, *51*(1-6), 733-741.
50. Lindahl, O. (1976). Mechanical properties of dried defatted spongy bone. Acta Orthopaedica, 47(1), 11-19.
51. Kutz, M. (2003). Standard handbook of biomedical engineering and design (pp. 8-1). McGraw-Hill.
52. Fondrk, M., Bahniuk, E., Davy, D. T., and Michaels, C. (1988). Some viscoplastic characteristics of bovine and human cortical bone. Journal of biomechanics, 21(8), 623-630.
53. RBurstein, A. H., Reilly, D. T., and Martens, M. (1976). Aging of bone tissue: mechanical properties. The Journal of Bone and Joint Surgery, 58(1), 82-86.
54. McCalden, R. W., McGeough, J. A., Barker, M. B., and Court-Brown, C. M. (1993). Age-related changes in the tensile properties of cortical bone. J Bone Joint Surg Am, 75(8), 1193-1205.
55. Praemer A, Furner S, Rice DP. Musculoskeletal conditions in the United States. Park Ridge: Am Acad Orthop Surg 1992. p. 1–85.
56. C.J. Damien, J.R. Parsons Bone graft and bone graft substitutes: a review of current technology and applications J Appl Biomater, 2 (1992), pp. 187–208
57. Peitl, Oscar, Edgar D. Zanotto, Francisco C. Serbena, and Larry L. Hench. "Compositional and Microstructural Design of Highly Bioactive P2O5–Na2O–CaO–SiO2 Glass-ceramics." Acta Biomaterialia 8.1 (2012): 321-32. Web.
58. Peitl, O., Dutra Zanotto, E., and Hench, L. L. (2001). Highly bioactive P2O5-Na2O-CaO-SiO2 glass-ceramics. Journal of Non-Crystalline Solids, 292(1-3), 115-126.
59. Hench, L. L. (1998). Biomaterials: a forecast for the future. Biomaterials, 19(16), 1419-1423.
60. Rahaman, M. N., Day, D. E., Sonny Bal, B., Fu, Q., Jung, S. B., Bonewald, L. F., and Tomsia, A. P. (2011). Bioactive glass in tissue engineering. Acta biomaterialia, 7(6), 2355-2373.

61. O'Donnell, M. D. (2012). Melt-Derived Bioactive Glass. Bio-Glasses: An Introduction, 13-27.
62. Zhou, Y., Li, H., Lin, K., Zhai, W., Gu, W., and Chang, J. (2012). Effect of heat treatment on the properties of SiO2–CaO–MgO–P2O5 bioactive glasses. Journal of Materials Science: Materials in Medicine, 23(9), 2101-2108.
63. Fu Q, Rahaman MN, Bal BS, Kuroki K, Brown RF. In vivo evaluation of 13-93 bioactive glass scaffolds with trabecular and oriented microstructures in a rat subcutaneous implantation model. J Biomed Mater Res 2010;95A:235–44
64. Jones JR, Poologasundarampillai G, Atwood RC, Bernard D, Lee PD. Nondestructive quantitative 3-D analysis for the optimization of tissue scaffolds. Biomaterials 2007;28:1404–13.
65. Jones JR, Ehrenfried LM, Hench LL. Optimizing bioactive glass scaffolds for bone tissue engineering. Biomaterials 2006;27:964–73.
66. Li WJ, Laurencin CT, Caterson EJ, Tuan RS, Ko FK. Electrospun nanofibrous structure: a novel scaffold for tissue engineering. J Biomed Mater Res 2002;60:613–21
67. Shin M, Yoshimoto H, Vacanti JP. In vivo bone tissue engineering using mesenchymal stem cells on a novel electrospun nanofibrous scaffold. Tissue eng 2004;10:33–41.
68. Jones, J. R. (2013). Review of bioactive glass: from Hench to hybrids. Acta biomaterialia, 9(1), 4457-4486.
69. Granito, R. N., Rennó, A. C., Ravagnani, C., Bossini, P. S., Mochiuti, D., Jorgetti, V., ... and Oishi, J. (2011). In vivo biological performance of a novel highly bioactive glass-ceramic (Biosilicate®): A biomechanical and histomorphometric study in rat tibial defects. Journal of Biomedical Materials Research Part B: Applied Biomaterials, 97(1), 139-147.
70. T. H. Courtney, Mechanical Behavior of Materials, McGraw-Hill, New York, 1990
71. Oonishi H. Interfacial reactions to bioactive and non-bioactive bone cements. In: Davies JE, editor. The bone biomaterial interface. Toronto: University of Toronto Press; 1991. p 321–333
72. Oonishi H, Kushitani S, Yasukawa E, Iwaki H, Hench LL, Wilson J, Tsuji E, Sugihara F. Particulate Bioglass compared with hydroxyapatite as a bone graft substitute. Clin Orthop Rel Res 1997;334:316–325.
73. Oonishi H, Hench LL, Wilson J, Sugihara F, Tsuji E, Kushitani S, Iwaki H. Comparative bone growth behavior in granules of bioceramic materials of various sizes. J Biomed Mater Res 1999; 44:31–43.
74. Bone Growth Into Spaces Between 45S5 Bioglass Granule. Oonishi, H. Kushitani, S.;Yasukawa, E. Kawakami, H. University of Turku;

Biomaterials Research Group; Abo Akademi University; Biomaterials Research Group BIOCERAMICS -CONFERENCE-; 7; 139-144; ISBN 0750621753

75. Oonishi, H., Hench, L. L., Wilson, J., Sugihara, F., Tsuji, E., Matsuura, M., ... and Mizokawa, S. (2000). Quantitative comparison of bone growth behavior in granules of Bioglass®, A-W glass-ceramic, and hydroxyapatite. Journal of biomedical materials research, 51(1), 37-46. (Class A and Class B)
76. http://solutions.3m.com/wps/portal/3M/en_US/EnergyAdvanced/Materials/Brands/Ceradyne/
77. http://www.hogentogler.com/sieve_shakers.asp
78. Bretcanu, O., Chatzistavrou, X., Paraskevopoulos, K., Conradt, R., Thompson, I., and Boccaccini, A. R. (2009). Sintering and crystallisation of 45S5 Bioglass< sup>®</sup> powder. Journal of the European Ceramic Society, 29(16), 3299-3306.
79. Standard test method for monotonic compressive strength of advanced ceramic at ambient temperature, ASTM designation C1424-10
80. Zhu, P., Masuda, Y., & Koumoto, K. (2004). The effect of surface charge on hydroxyapatite nucleation. Biomaterials, 25(17), 3915-3921.
81. Ma, X. H., Wu, L. M., Guo, X. Y., Zhang, M. H., & Ma, A. L. (2013). Methylene Blue Adsorption by Synthetic Nano-Carbon-Hydroxylapatite. Advanced Materials Research, 664, 326-330
82. Kokubo, T., Kushitani, H., Sakka, S., Kitsugi, T., & Yamamuro, T. (1990). Solutions able to reproduce in vivo surface-structure changes in bioactive glass-ceramic A-W3. Journal of biomedical materials research, 24(6), 721-734..
83. Thompson, I. D., and Hench, L. L. (1998). Mechanical properties of bioactive glasses, glass-ceramics and composites. Proceedings of the Institution of Mechanical Engineers, Part H: Journal of Engineering in Medicine, 212(2), 127-136.
84. Dutta, G., & Bose, D. (2012). Effect of Sintering Temperature on Density, Porosity and Hardness of a Powder Metallurgy Component. International Journal of Emerging Technology and Advanced Engineering Website. ISSN, 2250-2459.
85. Hashmi, M. U., Shah, S. A., Umer, F., & Alkedy, A. S. (2013). EFFECT OF SINTERING TEMPERATURE ON MICROSTRUCTURE AND IN-VITRO BEHAVIOR OF BIOACTIVE GLASS-CERAMICS. Ceramics–Silikáty, 57(4), 313-318.
86. Kazarian, S. G., Andrew Chan, K. L., Maquet, V., & Boccaccini, A. R. (2004). Characterisation of bioactive and resorbable polylactide/Bioglass<

sup>®</sup> composites by FTIR spectroscopic imaging. Biomaterials, 25(18), 3931-3938
87. Vallet-Regí, M., Romero, A. M., Ragel, C. V., & LeGeros, R. Z. (1999). XRD, SEM-EDS, and FTIR studies of in vitro growth of an apatite-like layer on sol-gel glasses. Journal of biomedical materials research, 44(4), 416-421.
88. Rehman, I., Knowles, J. C., & Bonfield, W. (1998). Analysis of in vitro reaction layers formed on Bioglass® using thin-film X-ray diffraction and ATR-FTIR microspectroscopy. Journal of biomedical materials research, 41(1), 162-166.
89. Notingher, I., Boccaccini, A. R., Jones, J., Maquet, V., & Hench, L. L. (2002). Application of Raman microspectroscopy to the characterisation of bioactive materials. Materials characterization, 49(3), 255-260.